Construction and Building Materials 483 (2025) 141821

Contents lists available at ScienceDirect

Construction and Building Materials

journal homepage: www.elsevier.com/locate/conbuildmat

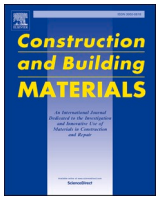

Effective restoration of reinforced concrete beams with severe stirrup corrosion using high-strength strain-hardening cementitious composites (SHCC)

Haroon Younas [a], Jing Yu [b,*], Christopher K.Y. Leung [a]

[a] Department of Civil and Environmental Engineering, The Hong Kong University of Science and Technology, Hong Kong, PR China
[b] Department of Civil Engineering, The University of Hong Kong, Hong Kong, PR China

ARTICLE INFO

Keywords:
Structural repair
Structural strengthening
Shear reinforcement
Steel corrosion
Strain-Hardening Cementitious Composites
Engineered cementitious composites
Finite element models

ABSTRACT

The corrosion of steel in reinforced concrete (RC) beams is a significant problem that can lead to premature structural failure. Specifically, shear stirrups with less concrete cover than flexural reinforcements are more vulnerable to early corrosion. Traditional repair techniques by attaching additional reinforcements to the corroded stirrups through lapping are time-consuming and costly. Moreover, achieving adequate lap length for effective stress transfer may not be feasible if the depth of the beam is limited. To solve the above issue, this study introduces an innovative repair technique using high-strength Strain-Hardening Cementitious Composite (SHCC). This material can sustain significant tensile/shear stress at elevated strain levels and then eliminate the need for stirrup lapping and extensive concrete removal. Four-point bending tests were performed on RC beams with a region (covering some adjacent stirrups) with a high percentage of stirrup area loss to simulate the severe situations, with and without a high-strength SHCC patch. Test results showed that the high-strength SHCC patch can effectively restore the ultimate load-bearing capacities to 96.12 % and 98.90 % of the full capacity of uncorroded beams for 50 % and 100 % stirrup losses, respectively. Finite element models were developed to simulate the behavior of both the reference and patched beams, and the numerical predictions satisfactorily matches the experimental outcomes. These findings demonstrate the effectiveness of using high-strength SHCC patch to restore the load-bearing capacity of RC beams with severe stirrup corrosion, thereby validating the practical applicability of this innovative repair technique.

1. Introduction

The long-term durability and serviceability of reinforced concrete (RC) structures in harsh environments are compromised by a multitude of deteriorative factors, including the corrosion of steel reinforcements [1–3]. Particularly in coastal cities like Hong Kong, rebar corrosion stands out as a pervasive and severe issue contributing to the decline of RC structures, necessitating advanced protective strategies and repair methodologies. The shear behavior of RC structures is influenced by a variety of factors, including the loading configuration, the shear span-to-depth ratio, and the type of structural element. The sudden and brittle nature of catastrophic shear failure in RC members necessitates designs with greater shear loading capacity than flexural, to preempt such failures [4]. Nonetheless, shear failures can still occur, particularly when shear stirrups are significantly corroded, making the repair of these elements crucial. Traditional repair techniques by attaching additional rebars to the corroded reinforcements through lapping are time-consuming and costly. Moreover, where the depth of the structural element is limited, achieving adequate lap length for effective stress transfer may not be feasible. In the literature, the most common techniques for strengthening the shear RC beams are externally-bonded fiber-reinforced polymer (FRP) [5–10] and near surface mounted

Abbreviations and symbols: RC, Reinforced concrete; D, Diameter of reinforcement; XD, Space on top of the rebar; C, Concrete cover; ECC, Engineered cementitious composites; SHCC, Strain-hardening cementitious composites; FRP, Fiber reinforced polymers; GFRP, Glass fiber reinforced polymers; f_c, Compressive strength MPa; $\sigma < 0.5$, Peak stress before 0.5 % strain MPa; F_{tu}, Tensile strength MPa; ε_u, Tensile strain capacity %; REF-F, Reference beam with full stirrup area; REF-R50, Reference beam with three stirrups with 50 % area loss; REF-R100, Reference beam with three stirrups with 100 % area loss; BP-50, Patched beam with three stirrups with 50 % area loss; BP-100, Patched beam with three stirrups with 100 % area loss.

* Corresponding author.
E-mail addresses: hyounas@connect.ust.hk (H. Younas), ceyujing@hku.hk (J. Yu), ckleung@ust.hk (C.K.Y. Leung).

https://doi.org/10.1016/j.conbuildmat.2025.141821
Received 27 October 2024; Received in revised form 9 April 2025; Accepted 14 May 2025
Available online 16 May 2025

reinforcement [9,11–21]. While both techniques offer advantages, they also present several challenges and limitations. Externally-bonded FRP faces issues such as bonding and debonding issue [22], limited shear capacity increase [23], vulnerability and environmental exposure [24], labor-intensive application [25], risk of fire damage [23] and aesthetic impact [24]. Similarly, near surface mounted reinforcement is limited by its applicability for thin sections [26], risk of debonding and slip [26], complex installation process [27], challenges with irregular shapes [27], sensitivity to grove quality [28], and higher material costs [29]. Such limitations highlight the need for more efficient and robust repair solutions.

Engineered/Strain-Hardening Cementitious Composite (ECC/SHCC), known for its exceptional ductility, and superior crack control capabilities [30–32], has been increasingly considered for repair and strengthening applications [33–40]. These properties position SHCC as a potential game-changer in addressing challenges associated with corroded shear reinforcements. SHCC have proven effective in extending the service life of aging structures and enhancing safety. Chen et al. [41] showed that using SHCC patches can effectively repair severely corroded concrete beams under flexure. Figueiredo et al. [42] demonstrated the efficacy of SHCC in enhancing the impact resistance of RC beams. Baraghith et al. [43] reported that using precast SHCC plates significantly improved both the ultimate load capacity and the ductility of RC dapped-end beams under shear. Hu et al. [44] integrated SHCC into the compression zone in RC beams, which significantly enhanced both the shear strength and deformability of the beams. Ellithy et al. [40] demonstrated that replacing weak concrete cover with SHCC in pre-stressed GFRP reinforced concrete beams significantly enhances both the ultimate load capacity and ductility. Figueiredo et al. [45] showed that strengthening RC beams under shear with SHCC can significantly improve the impact resistance and energy dissipation capabilities. He et al. [46] demonstrated that a 1-cm-thick layer of SHCC significantly enhances crack width control in RC beams. These examples underscore the versatility and effectiveness of SHCC materials in a wide range of construction and repair contexts, from enhancing the seismic resilience of high-rise buildings to facilitating rapid infrastructure repairs and improving the durability. Additionally, unlike FRP, which can be limited by poor fire resistance and the need for special surface preparation, SHCC excels in environments where fire resistance, durability, and ease of application are critical [47,48].

Additionally, a hybrid technique simultaneously using FRP and SHCC has also been introduced for strengthening RC beams [37,49–53]. The hybrid FRP-SHCC technique offers significant potential for improving the durability and strength of RC members when applied correctly. The addition of FRP increases the load-carrying capacity, particularly enhancing the flexural and shear strength, while also resisting corrosion, extending the structure's service life in harsh environments. Moreover, the combination of SHCC's high deformation capacity and FRP's high tensile strength results in improved flexural performance of RC beams. However, this hybrid technique also has limitations. The installation process is complex and requires precise bonding between FRP, SHCC, and the existing concrete, making it more labor-intensive and technically demanding than other strengthening techniques. The cost of materials and labor is also higher compared to conventional techniques. Although research results appear to be promising, the long-term performance of this system is not fully understood. FRP materials are sensitive to environmental factors such as high temperatures and UV exposure, potentially leading to degradation over time if not properly protected.

Therefore, exploring using high-strength SHCC alone, rather than commonly available techniques, offers significant advantages. High-strength SHCC provides exceptional ductility, superior crack control, and resilience against environmental degradation, making it an ideal material for strengthening RC members without the need for additional reinforcement like FRP. By simplifying the installation process, SHCC eliminates the complexities and costs associated with FRP application, leading to more efficient and cost-effective solutions.

In the repair of RC structures with SHCC, establishing a strong bond between the SHCC and steel reinforcements is essential. Fisher and Li [54], Otsuka et al. [55], Chen et al. [56] and Figueiredo et al. [42] demonstrated that SHCC maintains a robust bond with steel reinforcements, significantly outperforming ordinary concrete in terms of stress transfer ability and bond strength, even under high deformation and crack formation. This ensures enhanced structural integrity and durability in repair applications.

However, despite these advancements, challenges remain in applying SHCC for shear strengthening, especially in corroded RC beams. Existing studies often focus on flexural repairs or general strengthening applications, with limited attention to shear strengthening under severe stirrup corrosion. Moreover, traditional repair techniques, such as externally bonded FRP and near-surface mounted reinforcement, face issues like complex installation, environmental vulnerability, and limited shear capacity improvement. This study addresses these gaps by exploring the use of high-strength SHCC as a novel and efficient repair method for restoring the shear capacity of RC beams affected by severe stirrup corrosion.

To overcome the limitations of commonly available repair techniques for RC beams with severe stirrup corrosion, this study introduces an innovative repair technique using high-strength SHCC. This technique can eliminate the need for stirrup lapping and extensive concrete removal, thus offering a quicker and more cost-effective repair solution. The effectiveness of this repair technique was assessed through an experimental study on concrete beams, subjected to varying degrees of cross-sectional area loss (specifically, 0 %, 50 %, and 100 %) of a region (covering some adjacent stirrups) on one lateral side, with and without a high-strength SHCC repair patch applied over the affected area. These specimens were then tested under four-point bending to evaluate the shear capacity attainable through this repair technique. In parallel, a finite element model was developed simulate the behavior of both the reference and patched beams.

2. Four-point bending test of high-strength SHCC patched beams

2.1. Materials

The high-strength SHCC utilized in this study were developed by the authors [57], details of which are outlined in Table 1. With 2 vol% polyethylene fibers [58], this specific SHCC formulation achieves high tensile strength and strain capacity (Fig. 1) even 70 % of the Portland cement is replaced by supplementary cementing materials [59]. The concrete used for beam specimens was sourced from a local ready-mix concrete plant in Hong Kong. The beam specimens were reinforced with high-strength deformed steel rebars that conform to the CS2:2012 (Grade 500B) – Class 2 standard [60] for the flexural reinforcement, along with round steel stirrups employed as the shear reinforcement over certain sections of the beam.

The mechanical properties of the high-strength SHCC and concrete utilized in this investigation are compiled in Table 2, while the characteristics of the steel reinforcements, as provided by the supplier, are detailed in Table 3. A comparative analysis of the effect of curing conditions for high-strength SHCC (Table 2) indicates that the specimens cured using wet burlap exhibits slightly lower compressive strength, tensile strength, and tensile strain capacity than those under standard curing. However, curing with wet burlap is likely to better simulate the real condition encountered in practical applications.

2.2. Specimen preparation

To simulate relatively severe situations and make the experiments simple, a region (covering some adjacent stirrups) with 50 % and 100 % stirrup area losses is assumed in this study. The stirrups with reduced area were prepared by polishing. We introduce a L-shaped patch of high-

Table 1
Mix configuration of high-strength SHCC (mass ratio).

Binder			Fine silica sand	Water	Super-plasticizer[d]	Polyethylene fiber (vol%)
Cement[a]	Fly Ash[b]	Limestone Calcined Clay[c]				
0.3	0.3	0.4	0.3	0.2	2.07	2

[a] Type-I Portland cement (52.5 N as BS EN 197–1:2011).
[b] Class F (ASTM C618).
[c] Details on Limestone Calcined Clay can be found in [61,62]
[d] Polycarboxylate superplasticizer (solid content).

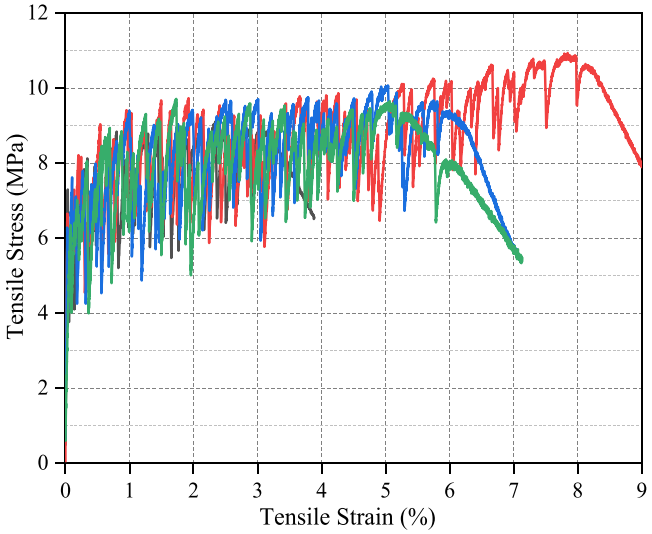

Fig. 1. Tensile stress-strain curves of high-strength SHCC under standard curing (after [14]).

strength SHCC (illustrated in Fig. 3) and aims at optimizing the repair process. The dimensions "D" and "C" in the design indicate the diameter of the longitudinal rebar and the thickness of concrete cover of the structural element, respectively. To ensure a complete encasement of the rebar with the repair material, a space "D" beyond the rebar is specified, facilitating proper bonding [63]. Additionally, an "xD" space above the rebar—where "x" is a variable yet to be determined—provides the necessary bond length for effective stress transfer. Opting for an L-shaped configuration over a standard rectangular design not only reduces the concrete removal and amount of repair material needed but also enhances the precision in estimating the required strength of the repair mortar.

An experimental analysis was conducted on 10 reinforced concrete beams, segmented into three distinct configuration types. Each beam measured 180 mm in width, 350 mm in depth, and 2100 mm in length, as depicted in Fig. 2**(a)**. To prevent flexural failures, the beams were reinforced with five ∅25 mm longitudinal rebars (Y25) for tension and two ∅25 mm longitudinal rebars (Y25) for compression. The detailed configurations of these test specimens are provided in Table 4. A consistent shear span/depth ratio of 2.5:1 was maintained across all specimens. Reference beams, labeled REF-F, REF-R50, and REF-R100 in Table 4, vary based on their stirrup areas—ranging from no patching to patches that represent 50 % and 100 % reduced stirrup areas—to serve as benchmarks for assessing the effectiveness of the SHCC patch configurations.

In contrast, BP-50 and BP-100 denote the patched beams, where patching with high-strength SHCC was applied to address 50 % and 100 % nominal area loss of the stirrups, respectively. The spacing between stirrups was uniformly maintained at 100 mm across both the strengthened (weak span) and un-strengthened (strong span) portions of each beam, ensuring consistency in the structural testing setup. During the four-point bending test, the shear force exerted on the two shear spans remained identical, a critical factor in assessing the effectiveness of the repair technique. To prevent potential failure across the un-strengthened span of the beam specimens, the shear reinforcements deployed differed in material and size: plain round mild steel stirrups of ∅8 mm (R8) were used for the weak span, while high-strength ribbed steel stirrups of ∅10 mm (Y10) were chosen for the strong span. This strategic variation is aimed at providing a differential strength profile across the beam spans. The stirrup arrangement for both the weak and strong spans, alongside the configurations for the reference and patched beams (REF-R50, REF-R100, BP-50, and BP-100), which all exhibited varying degrees of stirrup area loss, is illustrated in Fig. 2**(a)**. Notably, for the specimens categorized under REF-R50, REF-R100, BP-50, and BP-100, 3 stirrups on one side were specifically designated to simulate area loss, showcasing the experimental setup's attention to detail in replicating real-world structural challenges.

The design of the L-shaped high-strength SHCC patch is detailed in Fig. 3, where it was specifically utilized for reinforcing round ∅8 mm stirrups that experienced 50 % and 100 % area loss. The depiction of stirrups with reduced cross-sectional areas is provided in Fig. 4. For the reference beams designated as REF-R50 and REF-R100, concrete encapsulated the entire area. It's important to highlight that in constructing the steel framework for the BP-50 and BP-100 beams, a strategic placement of plastruct polystyrene foam blocks, mirroring the patch's shape, was employed on the lateral side of the cage. This

Table 3
Properties of steel reinforcements.

Type	Yield stress (MPa)	Tensile strength (MPa)	Young's modulus (GPa)
High-strength ribbed steel (longitudinal rebar)	585	610	200[a]
Plain round steel (stirrup)	335	530	200[a]

[a] as per the local code of practice CS2:2012 [60]

Table 2
28-day mechanical properties of high-strength SHCC and concrete.

Material (Curing Condition)	Compressive strength f_c (MPa)	Tensile performance			
		Peak stress before 0.5 % strain$^{\sigma}$< 0.5 (MPa)	Tensile strength f_{tu} (MPa)	Tensile strain capacity ε_{tu} (%)	Young's modulus (GPa)
SHCC (Standard curing)	75.90	6.64	9.95	5.80	35
SHCC (Wet burlap)	72.49	6.49	9.68	5.40	35
Concrete (Wet burlap)	70.25	NA	5.9	NA	25

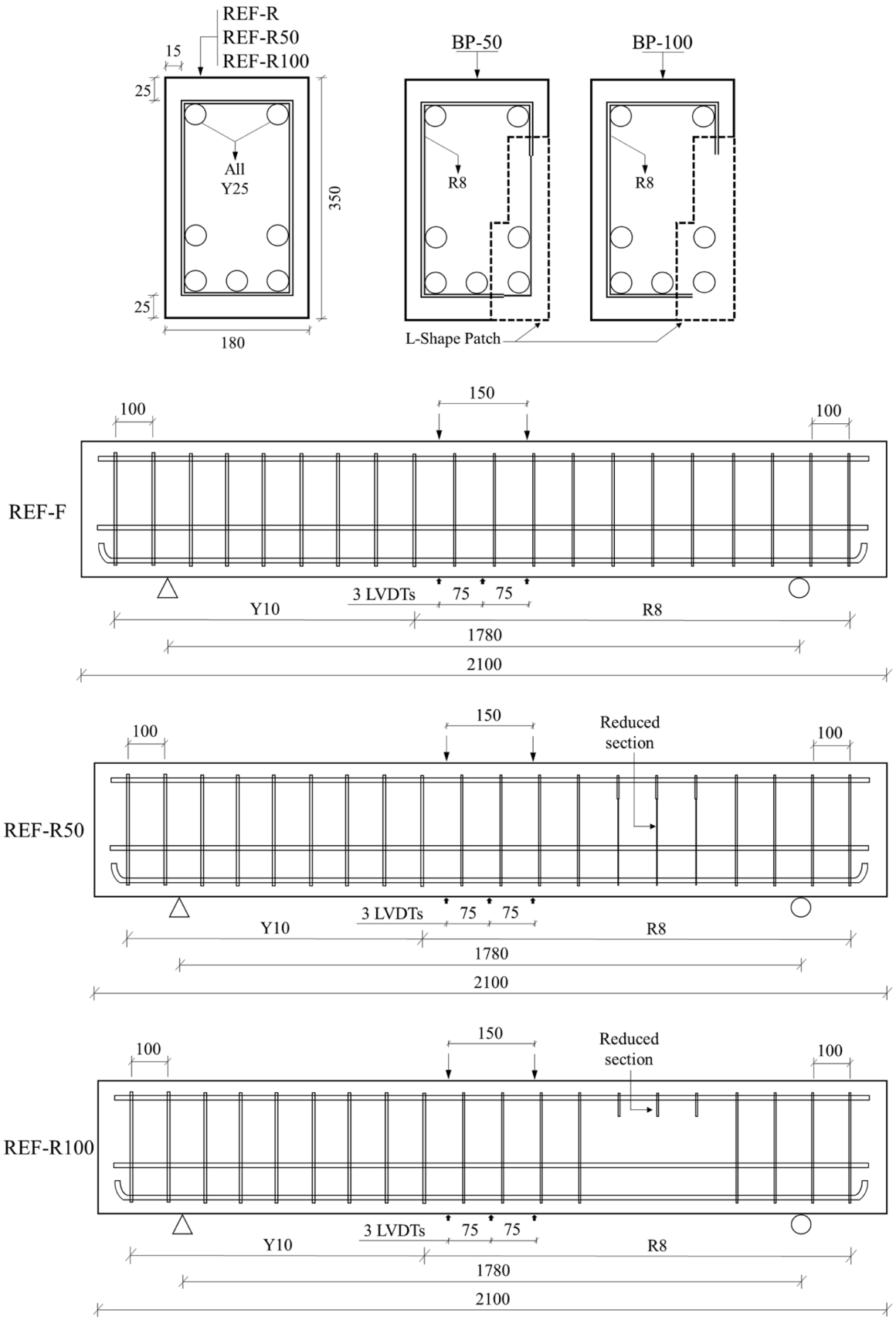

Fig. 2. Four-point bending test: (a) Beam specimen configurations (Units: mm), (b) Process flow chart, and (c) Test setup.

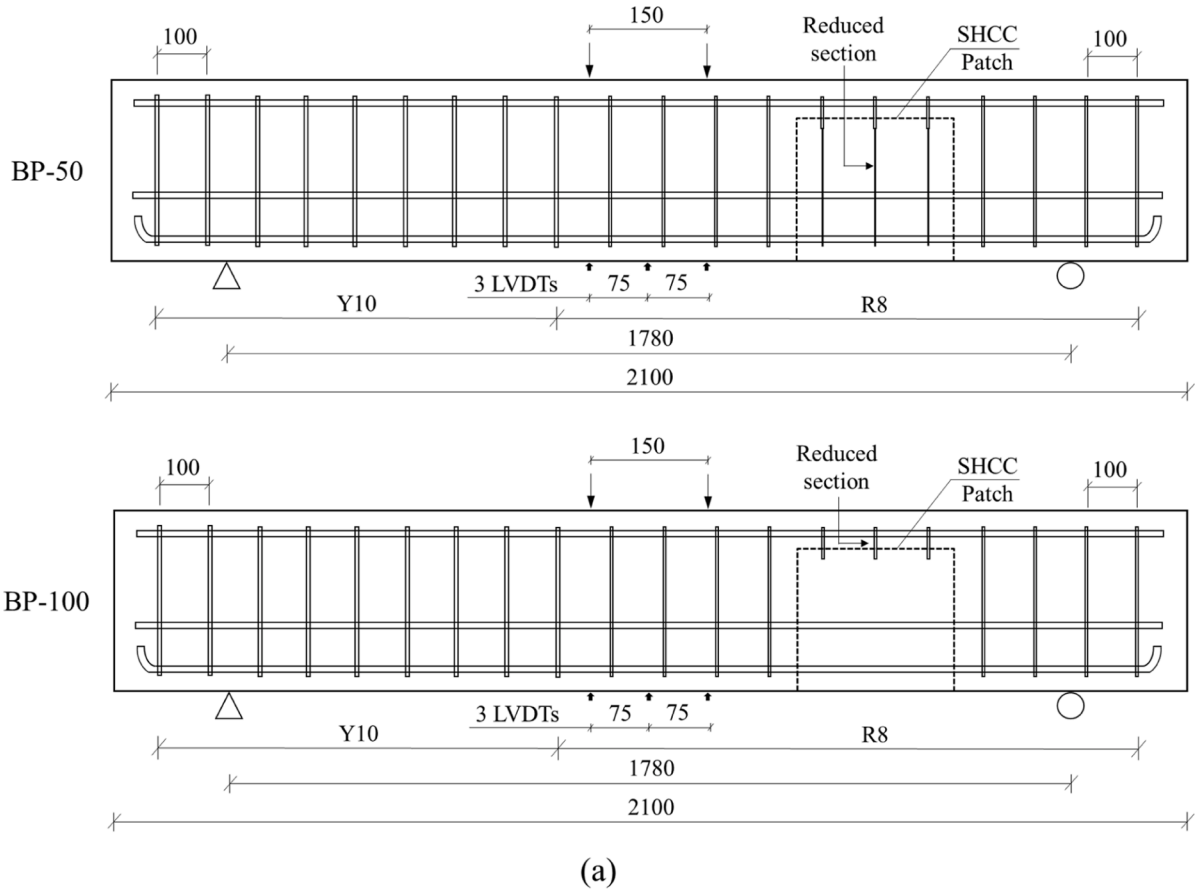

(a)

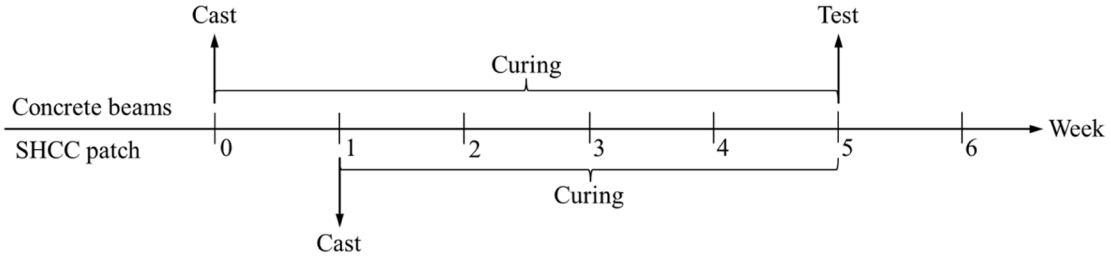

(b)

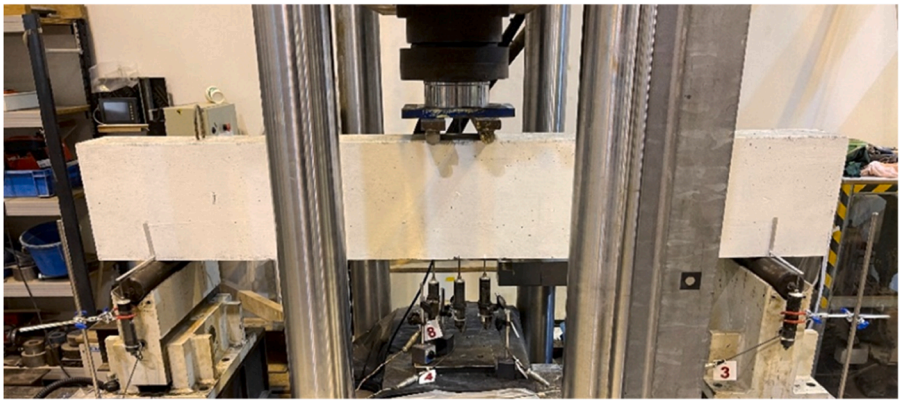

(c)

Fig. 2. (*continued*).

Table 4
Specimen arrangement for four-point bending beam.

Specimen type	Stirrup condition	Reduced area of each stirrup (%)	No. of stirrups with reduced area	Patch	No. of specimens
REF-F	Full Area	0	0	NA	2
REF-R50	Reduced Area	50	3	NA	2
REF-R100	Reduced Area	100	3	NA	2
BP−50	Reduced Area	50	3	Patching	2
BP−100	Reduced Area	100	3	Patching	2

technique was to reserve the necessary space for subsequent patch application. The procedural steps for specimen preparation are comprehensively illustrated in the process flow chart shown in Fig. 2**(b)**.

Following casting, all specimens, including the REF-F, REF-R50, and REF-R100 beams, alongside the concrete cubes and cylinders, were subjected to a 28-day curing period under wet burlap curing blankets in the laboratory, ensuring optimal conditions for concrete maturation prior to testing. After a curing period of 7 days, the BP-50 and BP-100 beam specimens were prepared for repair by removing the Plastruct polystyrene foam block. The concrete surface was then meticulously roughened using an air pressure hammer to expose the aggregate, enhancing the bond between the existing concrete and the SHCC patch, as illustrated in Fig. 4. All debris and dust were thoroughly removed to ensure a clean surface for the application of the high-strength SHCC patch. The specific high-strength SHCC was then prepared and cast into the designated voids left in the beam specimens BP-50 and BP-100. To maintain the necessary moisture content for curing, the patch area was covered with a polythene sheet. Following the application of the high-strength SHCC patch, the patched beam specimens BP-50 and BP-100 underwent a further 28-day curing process. This phase involved covering them with wet burlap curing blankets in the laboratory to ensure optimal moisture conditions for the curing of the SHCC patch before proceeding to testing.

Prior to the experimental and numerical testing phases, it's crucial to assess whether the SHCC repair patch can fully recover the load capacity lost due to corrosion in the stirrups. Considering the SHCC patch spans three adjacent stirrups, its total length is measured at 300 mm. The patch's smaller area, located above the longitudinal tensile reinforcements and perpendicular to the shear reinforcements, amounts to 15,000 mm² (calculated as 50 mm × 300 mm). Given the ∅8 mm

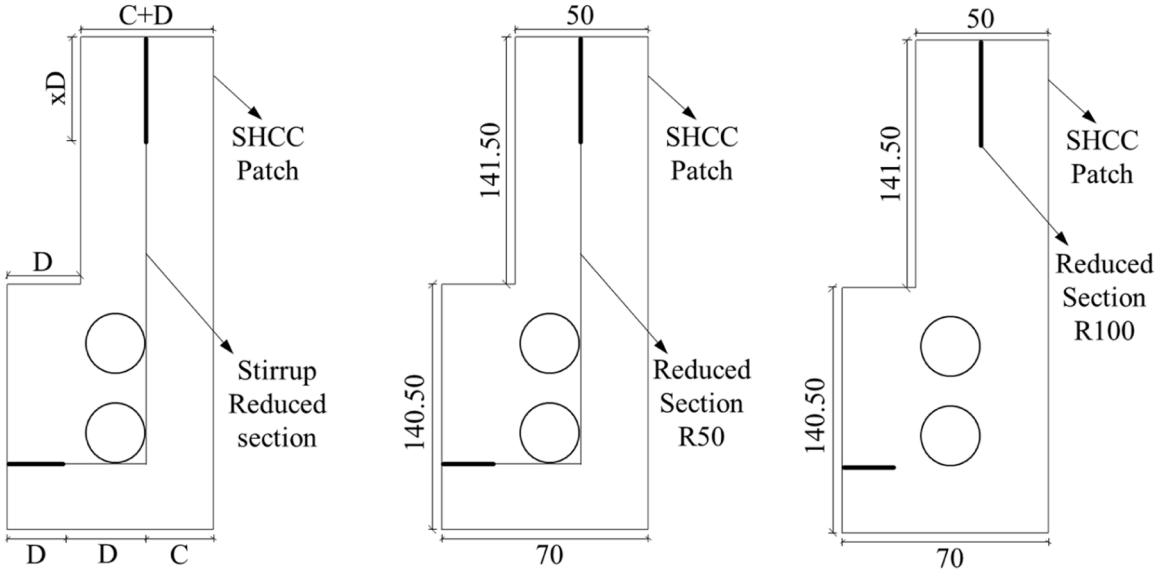

Fig. 3. General geometry of L-shape high-strength SHCC patching (Units: mm).

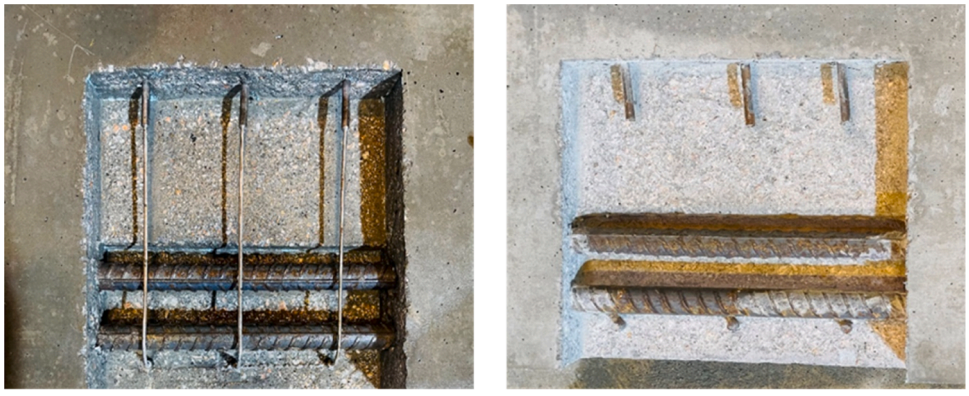

Fig. 4. Roughed surface of RC beam specimens; (a) BP-50 and (b) BP-100.

stirrup's yield strength of 335 MPa and assuming a complete loss of three adjacent stirrups, the SHCC's necessary strength to offset the load diminution is calculated as $3 \times 335 \times \pi \times (4\ mm)^2 / 15{,}000\ mm^2 = 3.37$ MPa. The specified high-strength SHCC mix is capable of bearing a stress of 6.64 MPa at strains below 0.5 %. Even with a conservative estimate accounting for a 40 % reduction in the SHCC's load-bearing capacity due to shear displacement across the crack, theoretical calculations suggest that full load capacity recovery of beams with fully corroded stirrups is achievable, provided the stress can be effectively transferred to the SHCC. This hypothesis will be thoroughly examined through the subsequent experimental and numerical analyses presented in this study.

2.3. Bending test setup

The structural beam specimens underwent testing using a four-point bending configuration on a 1000 kN DARTEC testing machine, as depicted in Fig. 2**(c)**. For these tests, the beams were designed with an effective depth of 325 mm and maintained a shear span/depth ratio of 2.5, equivalent to 815 mm. The beams were supported over a 1780 mm span, with loading points symmetrically positioned relative to the supports to create a constant moment zone of 150 mm at the center of each beam. The loading rate for all specimens was standardized at 0.6 mm/min. Testing terminated when the load notably declined to 85 % of the peak load observed. To accurately capture deflections at the beam's mid-span, three linear variable displacement transducers were strategically positioned.

2.4. Results and discussion

2.4.1. Load-deflection behavior

The results of the load-deflection behavior observed during the four-point bending test are detailed in Table 5, with Fig. 5 illustrating the relationship between load and mid-span deflection for all the beam specimens. The reference beam (REF-F) exhibited an average load-carrying capacity of 555.92 kN. When subjected to a 50 % and 100 % area loss in three adjacent stirrups, the beam specimens REF-R50 and REF-R100 demonstrated load capacities of 509.33 kN and 485.97 kN, respectively. These capacities represent 91.61 % and 87.41 % of REF-F's load-carrying ability. Remarkably, after undergoing repairs with high-strength SHCC, the patched beams BP-50 and BP-100 showed enhanced average load-carrying capacities of 534.36 kN and 549.83 kN, respectively, highlighting the effectiveness of SHCC in restoring structural integrity. Relative to the reference beam equipped with a full stirrup area, the ultimate load capacities of the patched beams (BP-50 (1), BP-50(2), and BP-100(1)) were restored to more than 96.42 %, 95.82 %, and 96.01 %, respectively. Notably, the BP-100(2) beam achieved full recovery of its ultimate load capacity. An intriguing observation from the study is the significant difference in load-carrying capacities between REF-R50 and REF-R100 beams; however, once repaired with the same high-strength SHCC patch, the repaired specimens, BP-50 and BP-100, exhibited a similar ability to bear loads prior to failure. This similarity suggests that the SHCC's enhanced strain-hardening capability, particularly in scenarios lacking steel stirrups, may play a crucial role, warranting further exploration.

2.4.2. Failure modes

Fig. 6 illustrates the cracking patterns observed in beams that did not undergo repair. The reference beam specimen REF-F, as shown in Fig. 6 **(a)**, exhibited a characteristic cracking pattern typical of members subjected to four-point bending tests. This included minor flexural cracks within the pure bending zone and the initiation of some diagonal shear cracks at the onset of testing. As the applied load was increased, these shear diagonal cracks expanded, while the longitudinal rebars effectively restrained the flexural cracks from widening in the pure bending region, showcasing the reinforcement's high yield stress. For the REF-F beams, failure was primarily due to shear tension within the beam's weaker span. At the point of ultimate load, concrete crushing was observed in the compression zone near the loading points of the beam specimens, with enlarged diagonal cracks appearing on the weaker side, extending between the loading area and the supports. The beams with reduced stirrup area, designated as REF-R50 and REF-R100, exhibited crack patterns similar to those of the REF series (Fig. 6**b and** Fig. 6**c)**). However, the presence of a specifically weakened region on one side of the beam, attributable to the diminished stirrup area, led to the yielding of the shear reinforcement. This was followed by the rapid development and spreading of cracks within the weaker span of the specimen. As depicted in Fig. 7 for REF-R100, the specimens with a reduced area of stirrups demonstrated the extension of shear cracks into a significant flexural crack under the weaker span and a bending crack on the beam's top surface over the weakened span.

For the beams repaired with patches (BP-50 and BP-100), the patterns of cracking are documented in Fig. 8**(a-f)** and Fig. 9**(a-f)**, with observations of beam and high-strength SHCC crack development at various loading stages (200 kN, 300 kN, 400 kN, and ultimate load) illustrated in Fig. 8**(a-f)** and Fig. 9**(a-f)**, respectively. At the initial 200 kN loading phase, each of the patched beam specimens exhibited only a few flexural cracks, along with the presence of fine diagonal

Table 5
Four-point bending results of beam specimens.

Specimen ID	Test Results				Simulation Results			Difference between Test and Simulation	
	Ultimate load (kN)	Mid-span deflection (mm)	Average ultimate load (kN)	Ultimate load recovery (%)	Ultimate load (kN)	Ultimate load recovery (%)	Mid-span deflection (mm)	Ultimate load (%)	Mid-span deflection (%)
REF-F(1)	584.04	8.18	555.92 ± 28.13	/	536.79	/	8.44	−3.44	9.39
REF-F(2)	527.79	7.25		/					
REF-R50 (1)	506.70	8.25	509.33 ± 2.63	91.14	513	95.56	7.41	0.72	−6.32
REF-R50(2)	511.97	7.57		92.09					
REF-R100(1)	496.14	6.97	485.97 ± 10.17	89.24	495.79	92.36	6.43	2.02	−4.24
REF-R100 (2)	475.79	6.46		85.58					
BP−50 (1)	536.04	10.57	534.36 ± 1.67	96.42	536.04	99.86	8.92	0.31	−14.39
BP−50(2)	532.69	10.27		95.82					
BP−100 (1)	533.79	8.26	549.83 ± 16.04	96.01	533.79	99.44	8.68	−2.91	−0.34
BP−100(2)	565.88	9.16		101.79					

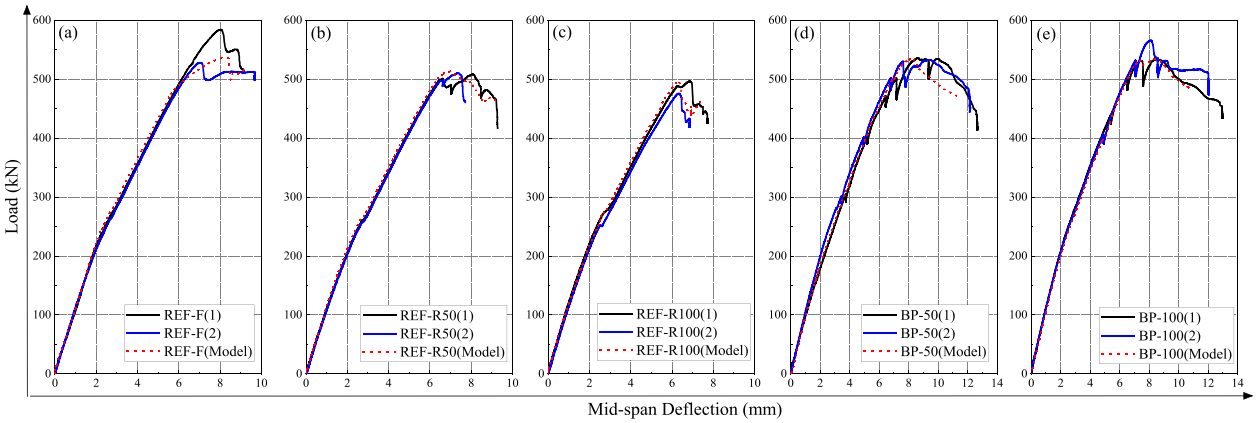

Fig. 5. Load versus mid-span deflection curves of testing and simulation beam specimens; (a) reference beam, (b) reference beam with 50 % reduced stirrup area, (c) reference beam with 100 % reduced stirrup area, (d) patched beam with 50 % reduced stirrup area, and (e) patched beam with 100 % reduced stirrup area.

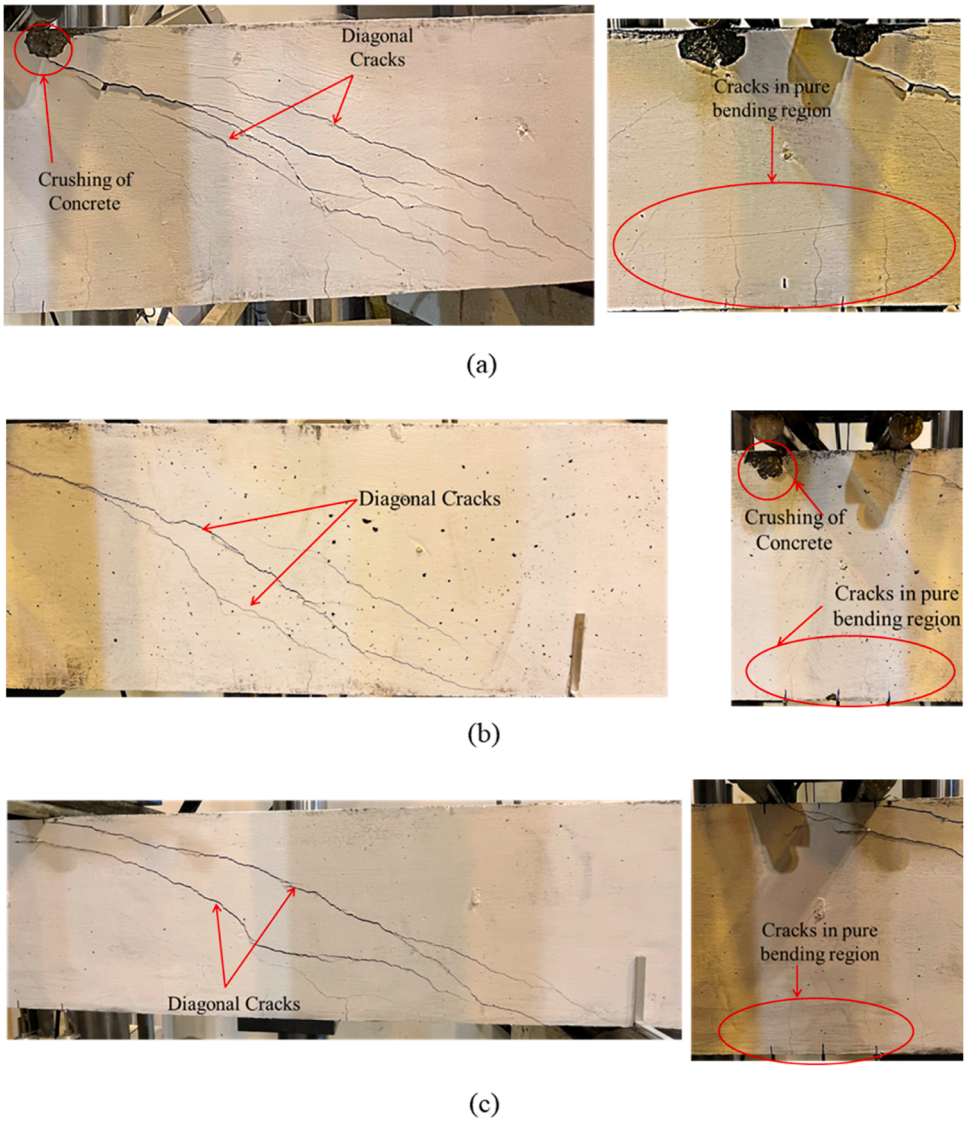

Fig. 6. Crack pattern of beam specimens; (a) REF-F, (b) REF-R50, and (c) REF-R100.

cracks in both BP-50 and BP-100 variants. Notably, the BP-50 beams showed no visible cracks on the high-strength SHCC patch at this stage. For the BP-100 beams, very fine cracks were detectable upon close examination, subsequently highlighted with a marker to enhance visibility for photographic documentation. As the loading increased, diagonal cracks began to extend within both the concrete and the high-

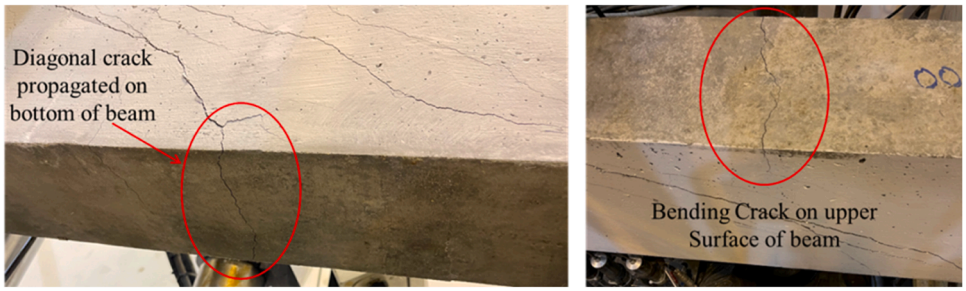

Fig. 7. Major cracks on the top and bottom surface of the REF-R100 beam specimen.

strength SHCC patches. Within the SHCC, the formation of multiple fine cracks with small openings was observed, diverging from the typical crack propagation seen in conventional concrete. Upon reaching the ultimate load, an extensive network of fine cracks was noticeable in the SHCC patch. However, failure predominantly manifested as a continuous shear crack stretching from the loading plate to the support. This was particularly evident after the yielding of the longitudinal reinforcement, where a significant shear crack appeared on the upper side of the patch, linking the support to the loading point. Concrete crushing within the compression zone near the loading point was also observed (as depicted in Fig. 8**(d)** and Fig. 9**(d)**). Following the attainment of the ultimate load, a bending crack on the top surface of the beam specimen was evident, as illustrated in Fig. 8**(e)** and Fig. 9**(e)**.

Additionally, a flexural crack on the beam's bottom surface was identified, connecting to the shear crack at the rear of the patch. To provide a comprehensive view, photographs were also captured of the opposite side, where full stirrup was present, since the beams were augmented only on one lateral side. The crack patterns observed at

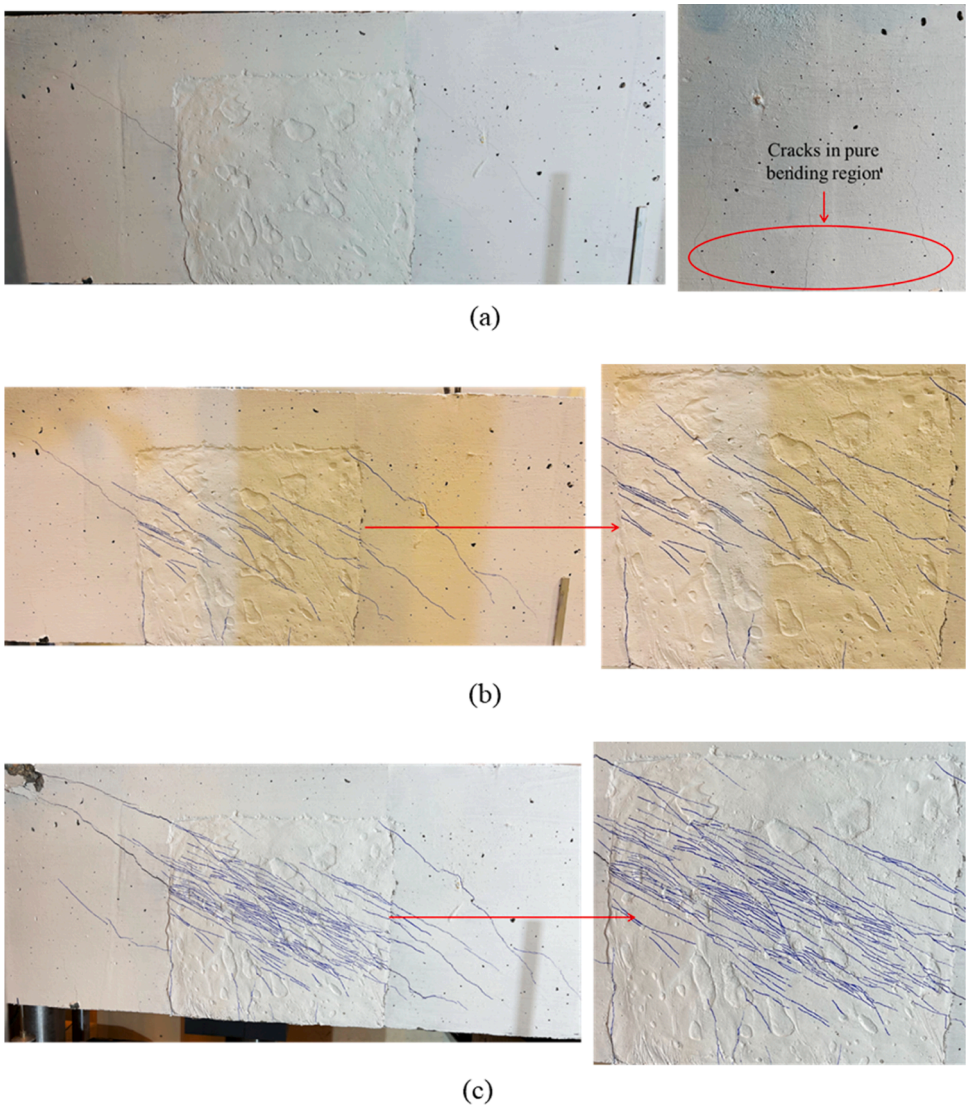

Fig. 8. Crack patterns of BP-50 at different loading points; (a) at 200 kN, (b) at 300 kN, (c) at 400 kN, (d) at ultimate loading, (e) bending cracks on the top and bottom surface of the beam, and (f) crack patterns on opposite to the strengthened side.

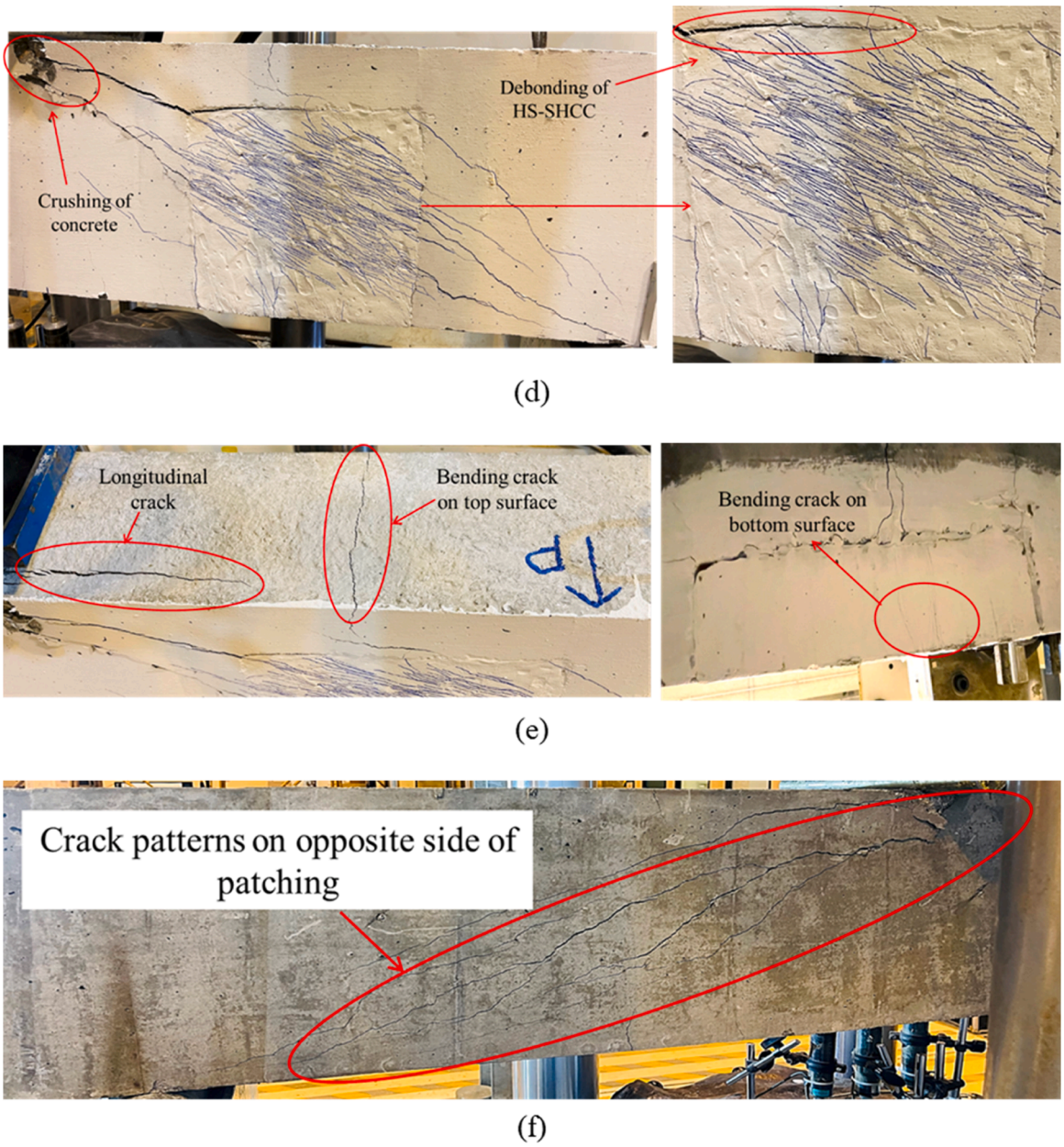

Fig. 8. (*continued*).

failure, as illustrated in Fig. 8**(f)** and Fig. 9**(f)**, bore resemblance to those seen in the unpatched REF-F beam specimens. Upon reaching the ultimate load, minor debonding between the substrate concrete and the high-strength SHCC was noted on the upper part of the patch in both BP-50 (Fig. 8**(d)**) and BP-100 (Fig. 9**(d)**) specimens. Notably, a more pronounced debonding crack was detected in BP-100 following the peak load, as shown in Fig. 9**(g)**. The high-strength SHCC in all repaired specimens exhibited multiple cracking behavior, characterized by numerous small openings without any significant cracks, even at the ultimate load. It was observed that the crack density within the high-strength SHCC might vary across specimens with identical configurations. A comparison between BP-50 and BP-100 specimens revealed a greater number of fine cracks in BP-100, where the absence of stirrups to resist shear forces led to more pronounced strain-hardening behavior of the SHCC patch. This suggests that the high-strength SHCC patch plays a more substantial role in enhancing the shear capacity of members that have experienced a complete loss of stirrup area.

3. Finite element modeling (FEM)

3.1. Simulation of tested beams with ABAQUS

The numerical analysis of RC beams with corroded stirrups and repaired using high-strength SHCC was conducted using a FEM software ABAQUS.

3.1.1. Constitutive models for concrete

In ABAQUS, modeling the nonlinear behavior of concrete materials necessitates a different approach than that used for steel reinforcement. The software offers three primary constitutive models for concrete: (1) the Cracking Model (CM), which focuses on the initiation and propagation of cracks; (2) Concrete Smeared Cracking (CSC), which distributes cracks over a wider area, and (3) Concrete Damage Plasticity (CDP), designed to simulate concrete's inelastic behavior under various loading conditions. This study utilizes the CDP model to characterize the complex inelastic behavior of concrete, including both compression and

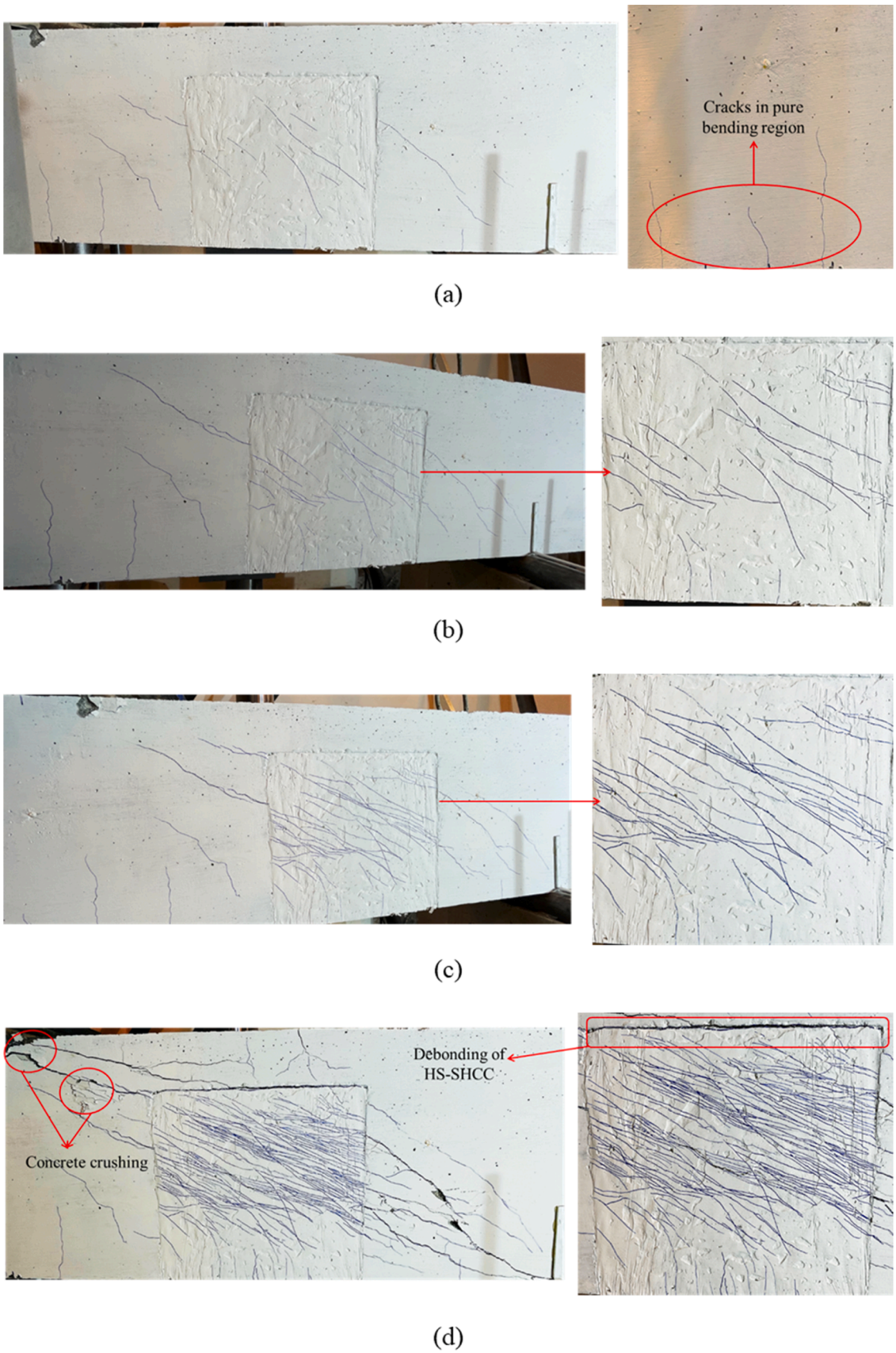

Fig. 9. Crack Patterns of BP-100 at different loading points; (a) at 200 kN, (b) at 300 kN, (c) at 400 kN, (d) at ultimate loading, (e) bending cracks on the top and bottom surface of the beam, (f) crack patterns on opposite to the strengthened side, and (g) debonding of high-strength SHCC.

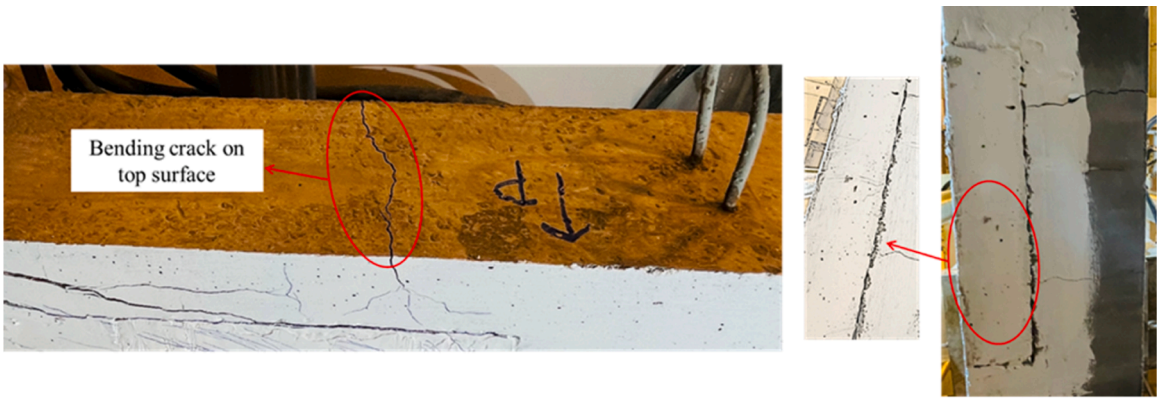

(e)

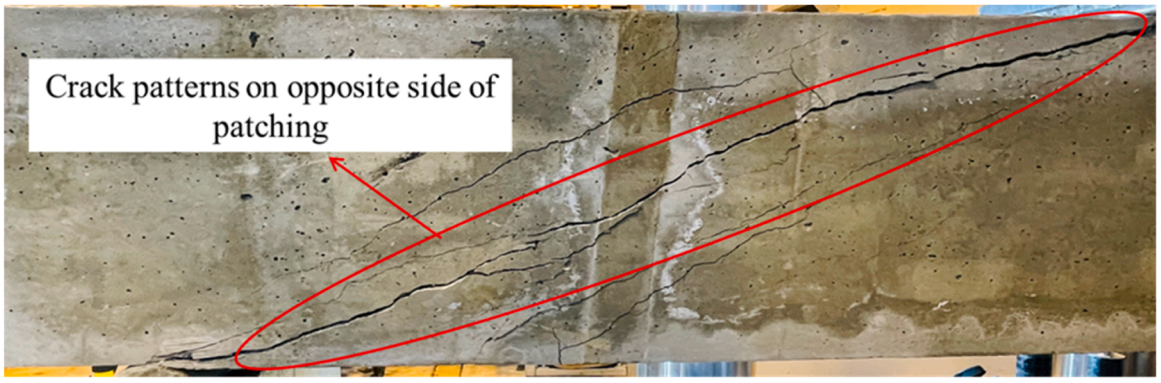

(f)

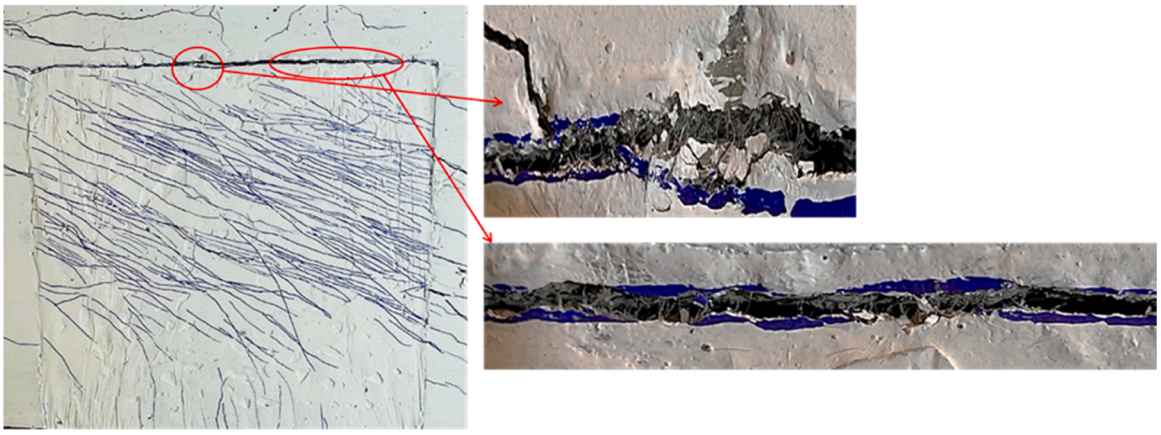

Fig. 9. (*continued*).

tension phases. Within the CDP model, stress-strain curves for concrete under both compressive and tensile states are defined by the user. Specifically, the tensile stress-strain relationship is modeled as linearly elastic up to the point of cracking, followed by a bi-linear post-peak response. To simplify the simulation, damage variables in both tension and compression were omitted, as they have negligible impact on the structural response under monotonic loading conditions. Although ABAQUS does not provide a specific material model for SHCC, the CDP model's versatility allows for the simulation of SHCC by incorporating its distinctive tensile strain-hardening behavior observed prior to softening post-ultimate strength. This adaptability of the CDP model makes it suitable for simulating both traditional concrete and innovative materials like SHCC, thereby offering a comprehensive tool for analyzing the behavior of reinforced concrete structures under a variety of conditions.

In the modeling process within ABAQUS for high-strength SHCC, the typical stress-strain curves for both tension and compression are simplified into multi-linear formats for ease of input. For the CDP model configuration specific to high-strength SHCC, the dilation angle—indicative of the volume change when the material undergoes shear loading—was set to 15 degrees. This assumption is based on the fact that SHCC lacks coarse aggregate, and such an angle aligns closely with empirical findings, offering numerical results that closely mirror experimental observations [64]. In contrast, the recommended dilation angle for conventional concrete is between 30 and 40 degrees, reflecting the presence of coarse aggregates in its composition [65]. To enhance the convergence of the CDP model, particularly when simulating high-strength SHCC, a minimal viscosity parameter of 0.0005 was

adopted, following the guidance of Barth and Wu [66]. The rest of the parameters were maintained at their default settings, as typically used for concrete simulations. Fig. 10 shows the constitutive models for concrete and high-strength SHCC. Steel reinforcements within the model were represented using a bi-linear elastic-plastic approach. The Poisson's ratio for the steel reinforcement was set to 0.3, encapsulating the material's deformation characteristics under load. Critical parameters such as yield stress, maximum stress, and Young's modulus for both high-yield and mild steel types were detailed in Table 3. To accurately integrate the steel reinforcement within the concrete matrix in the simulation, the 'embedded region constraint' feature was utilized. This approach ensures that the steel reinforcements are seamlessly incorporated into the host RC model, allowing for a realistic representation of their interaction and the overall structural behavior under various loading conditions.

3.1.2. Bond behavior between substrate concrete and high-strength SHCC

The interaction between substrate concrete and high-strength SHCC plays a crucial role in the effectiveness of the repair system. Experimental studies have consistently demonstrated that the bond strength between substrate concrete and SHCC is sufficiently robust, negating the necessity for any additional cohesive materials to facilitate their interaction [56]. In the simulation environment of ABAQUS, this robust interfacial bond is replicated by embedding the high-strength SHCC model within the steel reinforcement and RC matrix to ensure a seamless bond, utilizing the TIE CONSTRAINT ELEMENT for this purpose. Tie constraints in ABAQUS effectively prevent any relative movement between the connected materials, ensuring that the concrete model and SHCC patch behave as a unified entity within the simulation. While the tie constraint was used to replicate a perfect bond for numerical stability and computational simplicity, experimental results indicated some debonding at the interface between the SHCC and the concrete under loading conditions. This simplification may influence the predicted stress distribution and load-carrying capacity of the model. Incorporating an imperfect bond, such as through cohesive zone modeling or contact elements, could better capture the influence of debonding and provide more realistic insights into the behavior of the repair system. Future work will focus on incorporating these aspects to further refine the numerical simulations. This technique allows for the accurate representation of the composite action between SHCC and the existing concrete structure, mirroring the strong bond observed in practical applications. Further, the literature supports the premise of an effective bond between SHCC and steel reinforcement. Reflecting this, the ABAQUS model operates under the assumption that there is no slippage at the interface between the rebar/stirrup and SHCC, which theoretically maximizes the force transfer capabilities to the SHCC. This approach aims to provide an optimistic scenario regarding the load transfer efficiency and structural integrity of the repaired system, contributing to a more comprehensive understanding of the potential performance of SHCC as a repair material.

3.1.3. Model building and element type

The modeling of the concrete beam and high-strength SHCC patch utilizes eight-node brick elements (C3D8R), equipped with reduced integration to enhance computational efficiency. The steel reinforcement framework, encompassing both the longitudinal rebars and shear stirrups, is accurately represented through linear 3D truss elements employing a two-node system (T3D2). Upon assembling the various elements, the constraint module is engaged to seamlessly integrate the steel reinforcement within the concrete model, effectively designating the concrete as the host element. To accurately simulate the physical setup, loading plates and supports are constructed using an elastic

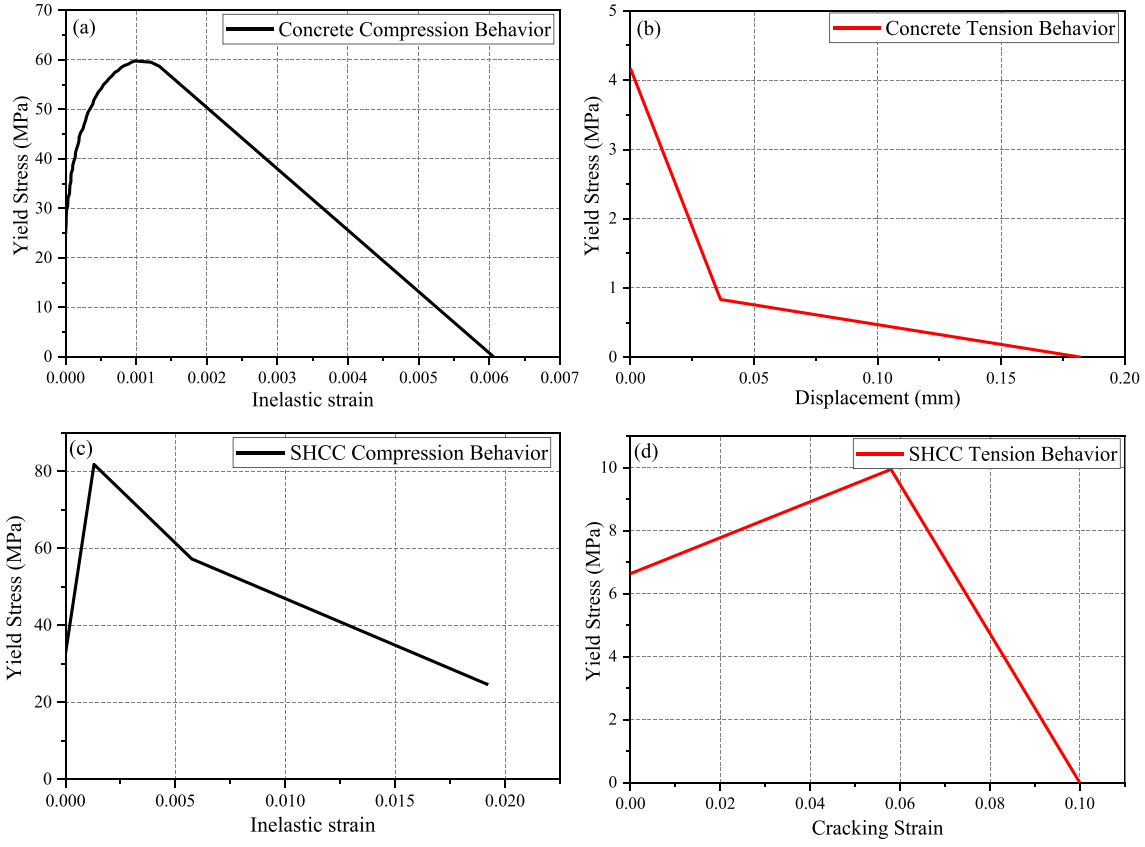

Fig. 10. Constitutive model curves: (a-b) for Concrete and (c-d) for high-strength SHCC.

material model for steel. Their interfaces with the concrete model are securely tied, ensuring there is no relative movement at the boundaries and thereby mitigating stress concentrations at critical points such as the loading areas and supports. Datum planes are strategically established for the precise placement of loading plates and support steel rods. Additionally, the interface between the high-strength SHCC patch and the underlying concrete substrate is meticulously joined using the tie constraint feature, ensuring a unified and integrated surface that accurately reflects the robust interfacial bond observed in experimental studies.

The model was configured to emulate a simply supported beam by applying boundary conditions along the center line of the supports. A reference point was established at the center of the loading plate and was coupled to the side nodes along the loading lines to ensure uniform load distribution. A prescribed downward displacement was then applied to this reference point to simulate the loading conditions. The entire assembly, including the elements representing the concrete beam, high-strength SHCC patch, steel reinforcement, loading plate, and supports, was meshed using the default mesh size to ensure adequate resolution for accurate stress and deformation analysis. Following the setup, the simulation job was submitted and closely monitored for any potential errors during the analysis process. The resulting beam model, incorporating the high-strength SHCC patch, is depicted in Fig. 11. Fig. 11**(a)** illustrates the entire beam assembly, showcasing the positioning of the loading and support plates. Fig. 11**(b)** and Fig. 11**(c)** provide detailed views of the patched region, highlighting the scenarios with 50 % and 100 % loss of steel reinforcement, respectively. These visualizations offer insights into the structural integration of the SHCC patch within the beam and its potential impact on reinforcing the damaged sections.

3.2. Verification between numerical and experimental results

3.2.1. Load-deflection relationships

Fig. 5 presents a comparison of the load-deflection curves obtained from both FEM simulations and experimental tests for these reference beams. The FEM results demonstrated a high degree of correlation with the actual experimental outcomes, particularly in depicting the ascending curves leading up to the ultimate load. Table 5 summarizes key performance metrics including maximum deflection (in mm), ultimate loading capacity (in kN), the percentage of ultimate load recovery for the beam specimens and difference (%) between simulation and testing specimens. Specifically, for the BP-50 beams, the simulated load-carrying capacity was within a 1 % margin of error compared to the experimental data, though the difference in deflection was more pronounced at approximately 15 % (Table 5).

Fig. 5 and Table 5 underline the effectiveness of the FEM in closely approximating the physical behaviors of the beam specimens under load. These outcomes, both experimental and numerical, underscore the effectiveness of employing high-strength SHCC for repairing beams with significantly corroded stirrups. The high percentage of load recovery observed indicates that SHCC repairs can nearly restore the structural capacity of corroded reinforced concrete beams to their original strength, highlighting SHCC's potential as a robust repair material in structural engineering applications.

3.2.2. Failure modes

Fig. 12 illustrates the failure modes of simulated models across all five examined cases, highlighting areas of higher stress and larger deformation, particularly on the right-hand side where stirrups are smaller (which may even be corroded). These simulations align with experimental observations, predicting failure predominantly on the beam's weaker side. Intriguingly, both experimental and simulation

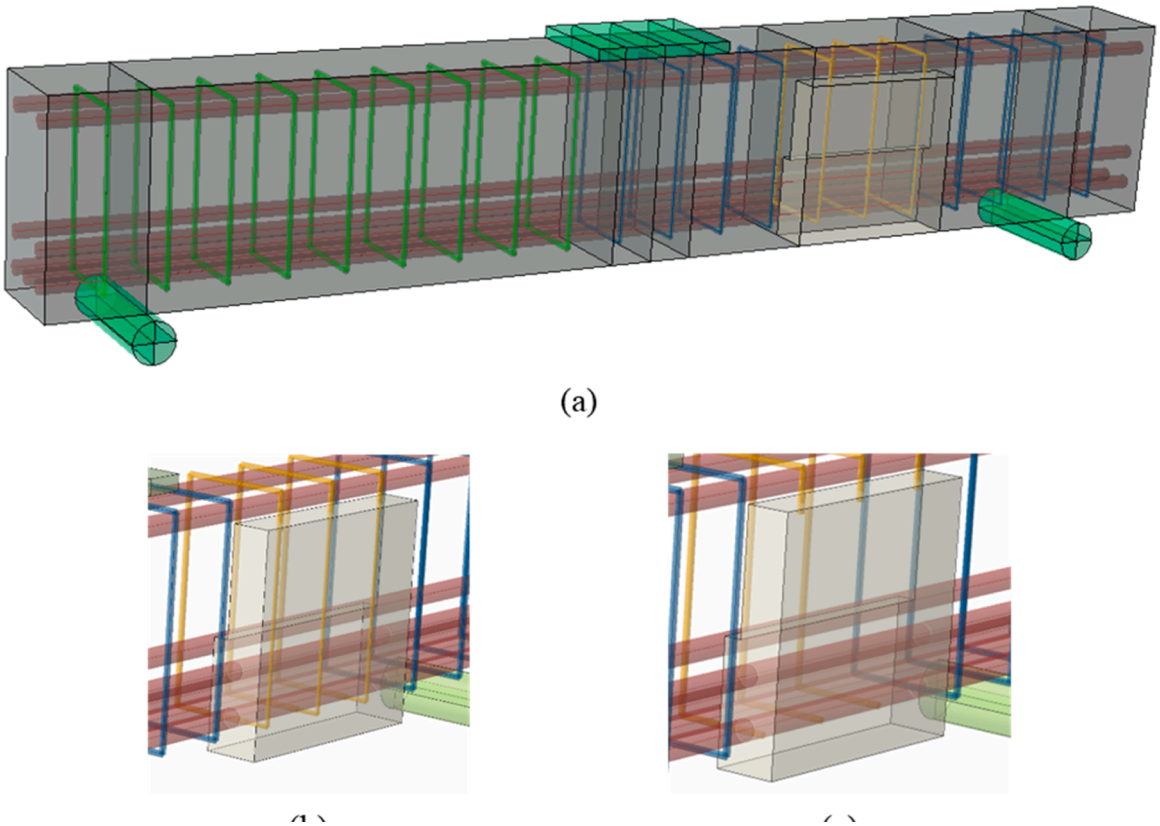

Fig. 11. Finite element model of the reinforced concrete beam with patch; (a) RC + high-strength SHCC model, (b) high-strength SHCC with 50 % reduced stirrup area, and (c) high-strength SHCC with 100 % reduced stirrup area.

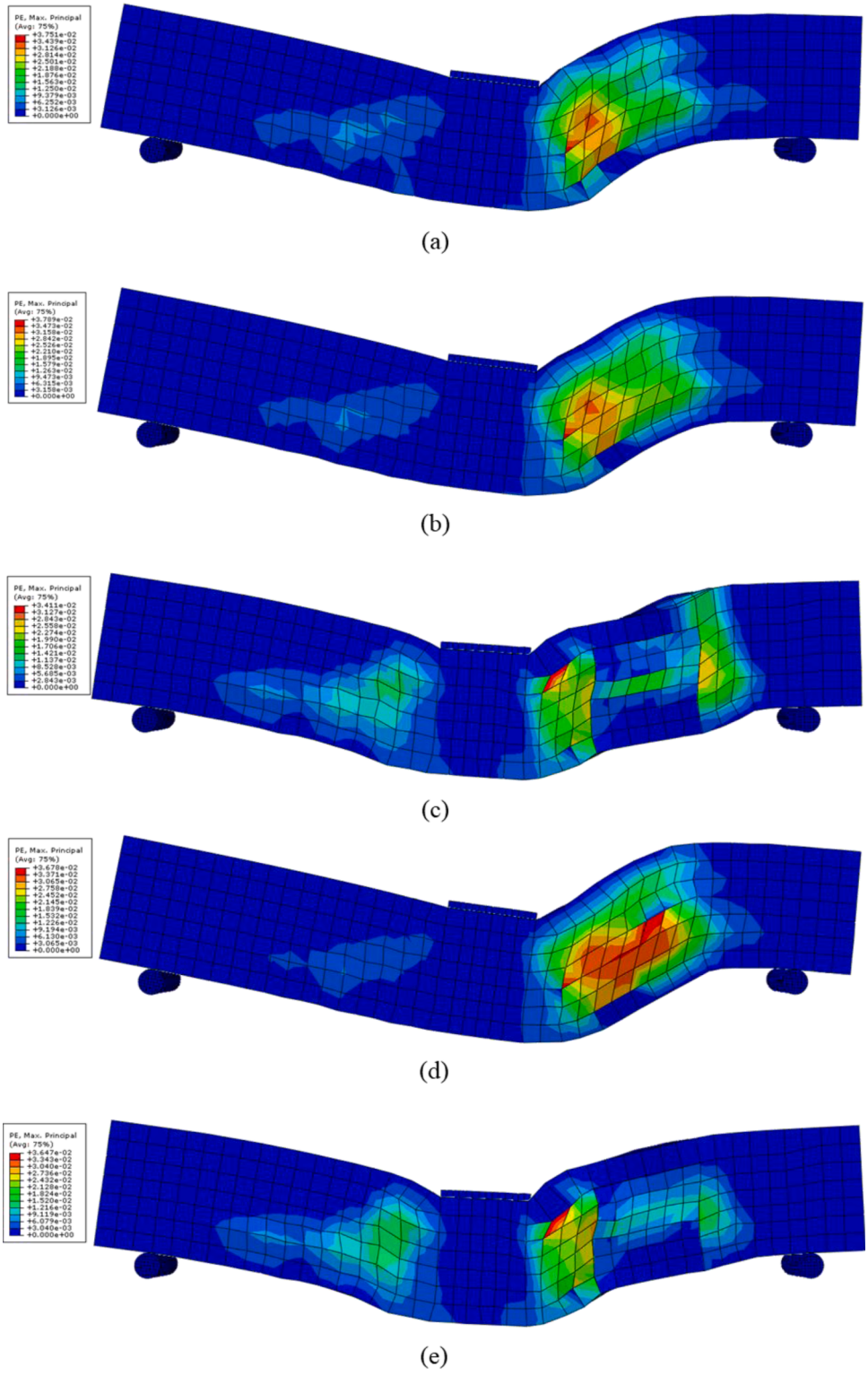

Fig. 12. Deformed shape of models: (a) REF-F(Model), (b) REF-R50(Model), (c) BP-50(Model), (d) REF-R100(Model), and (e) BP-100(Model).

results indicate that beam specimens BP-50 and BP-100, despite varying degrees of stirrup corrosion and being reinforced with identical high-strength SHCC patches, exhibit comparable load-bearing capacities up to the point of failure. To delve deeper into this phenomenon, Fig. 13 and Fig. 14 display the stress distribution within steel reinforcements and the high-strength SHCC patch across different loading stages (200 kN, 300 kN, 400 kN, ultimate load, and at the point of failure) for the BP-50 and BP-100 models, respectively.

In the analysis of the high-strength SHCC patch, the vertical stress component, which acts in opposition to the shear force, is visualized using color contours. These stress plots demonstrate a progressive pattern of high stress initiation on the right-hand side of the patch, extending towards the left as the load increases from (a) to (d). Notably, the upper right-hand corner of the patch bears the highest vertical stress. This pattern aligns with experimental findings, where the predominant shear crack in the concrete traverses through the SHCC patch in this

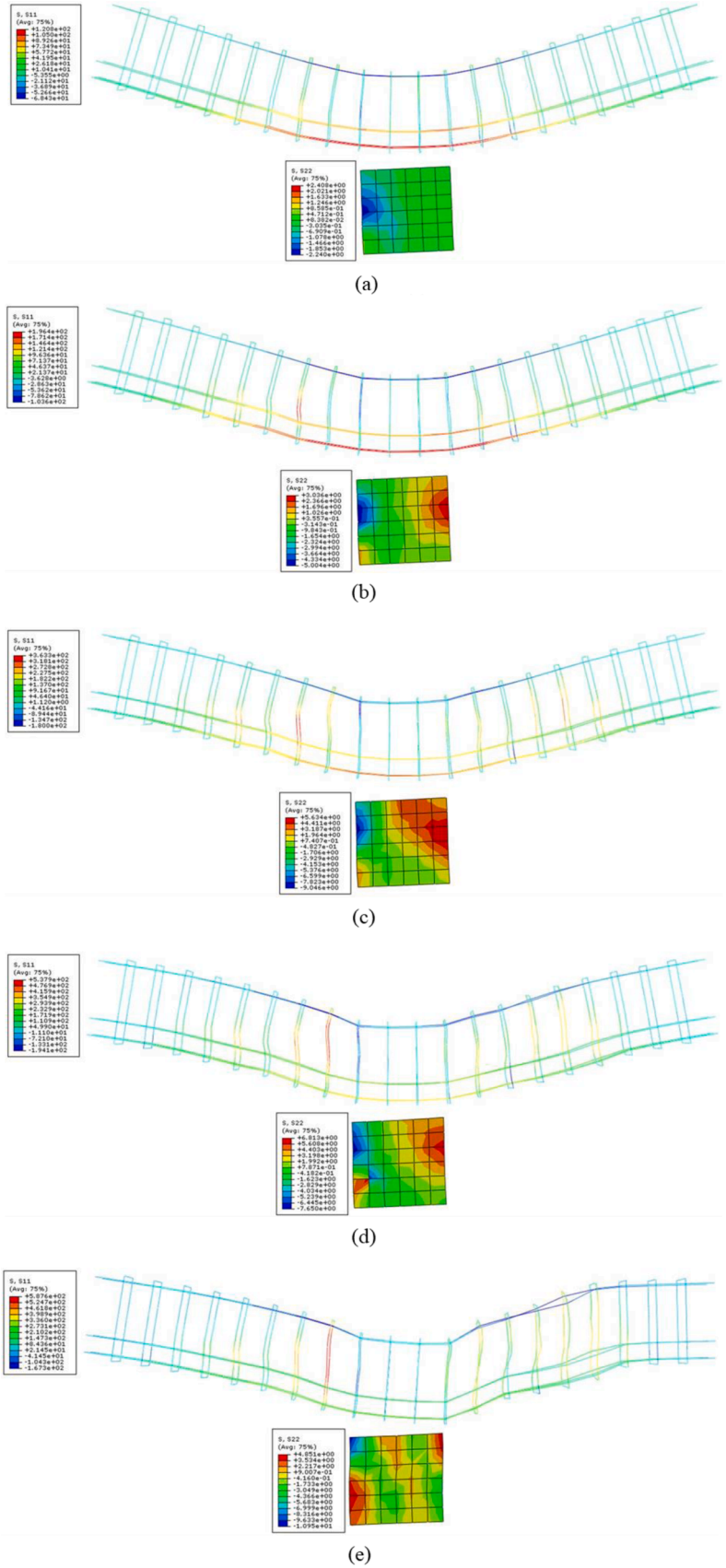

Fig. 13. Stress distribution in steel reinforcements and high-strength SHCC patch at different load levels for BP-50(Model): (a) 200 kN, (b) 300 kN, (c) 400 kN, (d) at ultimate load, and (e) at failure; color bar indicates vertical stress distribution, with abrupt color changes highlighting localized stress concentrations.

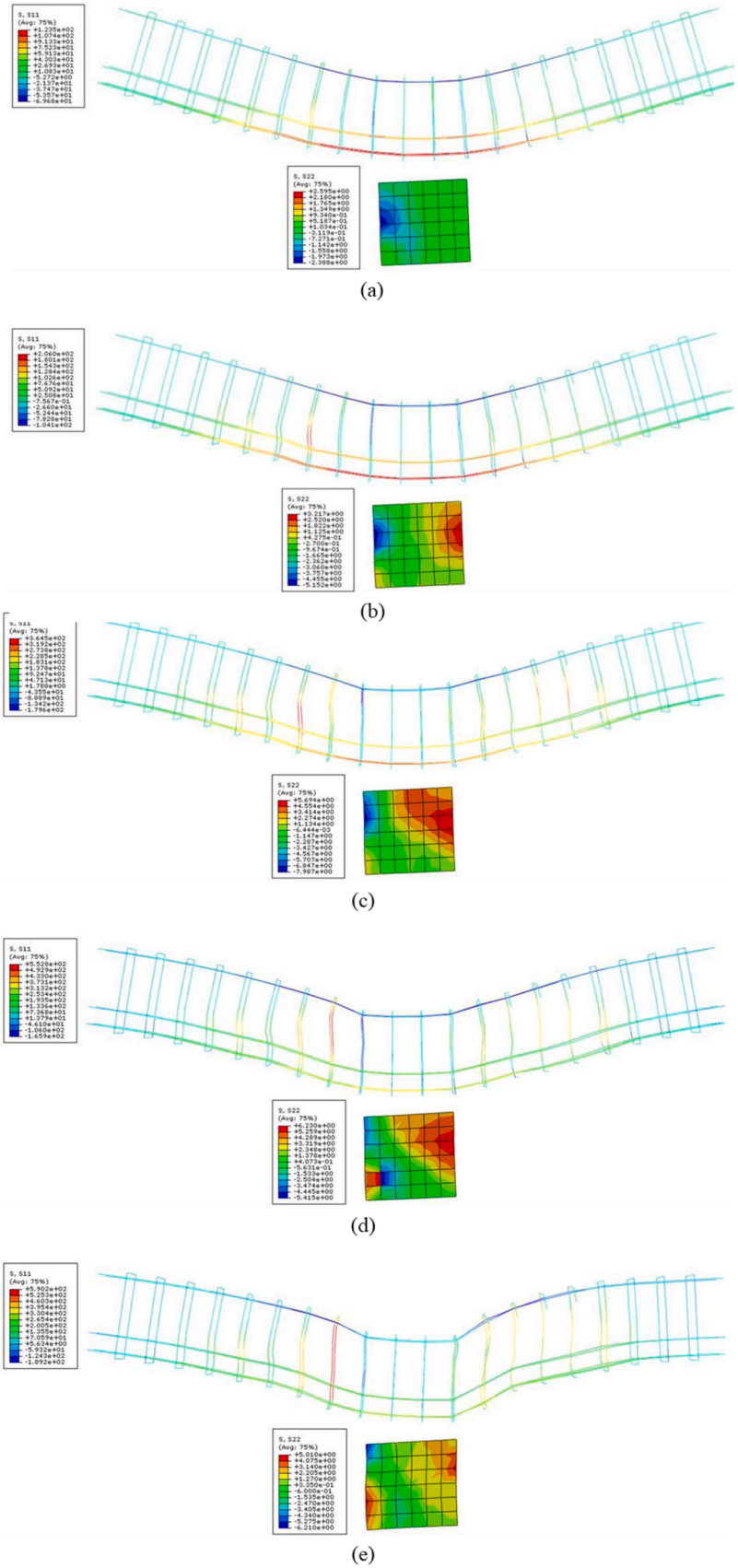

Fig. 14. Stress distribution in steel reinforcements and high-strength SHCC patch at different load levels for BP-100(Model): (a) 200 kN, (b) 300 kN, (c) 400 kN, (d) at ultimate load, and (e) at failure; colors represent stress magnitude, abrupt transitions indicate stress concentrations rather than discontinuous displacements.

specific area. Fig. 13**(d)** and Fig. 14**(d)** showcase the stress distribution at ultimate load for the BP-50 and BP-100 specimens, respectively. In these figures, areas depicted in yellow (and any hues representing values above this threshold) indicate stresses surpassing 1.992 MPa for BP-50 and 2.348 MPa for BP-100. A comparative analysis of these visuals reveals that a more substantial portion of the SHCC patch in BP-100 is subjected to high vertical stress. This observation sheds light on the comparable ultimate load capacities of BP-50 and BP-100, despite the latter experiencing complete corrosion of shear stirrups within the patched region. The FEM assumed a perfect bond between the SHCC patch and the substrate concrete, as described in the methodology. However, experimental results showed evidence of debonding at the interface under high loading conditions, particularly in specimens BP-100, as shown in Fig. 9(g). This debonding could affect the stress transfer efficiency and load redistribution within the repaired beams. While the perfect bond assumption provides an optimistic scenario for modeling, incorporating a more realistic representation of the interface, such as cohesive zone models or contact elements, could better capture the influence of debonding on structural performance. Future studies should consider these approaches to further refine the numerical model and explore the effects of an imperfect bond on stress distribution and failure mechanisms.

The color bars shown in Fig. 12, Fig. 13 and Fig. 14 represent the magnitude of vertical stresses developed within the high-strength SHCC patches and steel reinforcements. Regions with abrupt changes or apparent discontinuities in the color bar do not imply actual discontinuous displacement or structural separation. Rather, these sharp gradients highlight localized areas of stress concentration, particularly around the interfaces between materials or at areas with reduced stirrup reinforcement. The distinct boundaries in colors, particularly evident in Fig. 12 (c) and (d), correspond to stress transitions arising from the modeled material behavior and stress redistribution, reflecting the realistic and localized stress responses in the finite element analysis.

4. Conclusions

This study explored the feasibility of using high-strength SHCC to restore the load-carrying capacity of RC beams with severe stirrup corrosion. Four-point bending tests and finite element simulations were performed on RC beams (with a span/depth ratio of 2.5) with a region (covering some adjacent stirrups) with a high percentage of stirrup area loss to simulate the severe situations, with and without a high-strength SHCC patch. Test results showed that the high-strength SHCC patch can effectively restore the ultimate load-bearing capacities to 96.12 % and 98.90 % of the full capacity of uncorroded beams for 50 % and 100 % stirrup losses, respectively. Compared with the reference beams, including those with full capacity (full stirrup area) and with reduced capacity (reduced stirrup area but not repaired), the proposed repair technique can effectively restore the ultimate load-bearing capacities to 96.12 % and 98.90 % of the full capacity of uncorroded beams for 50 % and 100 % stirrup losses, respectively, without adding any new steel reinforcements. Additionally, the numerical results from finite element simulations for all the beam specimens were in satisfactory agreement with the experimental results. These findings demonstrate the effectiveness of using high-strength SHCC patch to restore the load-bearing capacity of RC beams with severe stirrup corrosion. The proposed technique can reduce the required amount of concrete to be removed for steel lapping and the associated time and cost.

While this study provides valuable insights, certain limitations should be acknowledged. The experiments were conducted under controlled laboratory conditions, and the long-term performance of the repair under field conditions was not addressed. Therefore, future research can focus on field validations to assess the scalability and durability of the SHCC repair technique under real-world conditions. Refining the finite element model to account for debonding at the interface between SHCC and substrate concrete is another critical area of future work.

The findings and proposed future directions highlight the potential of SHCC as a robust and versatile solution for structural rehabilitation, addressing the challenges posed by aging infrastructure and ensuring long-term performance under diverse conditions.

CRediT authorship contribution statement

Jing Yu: Writing – review & editing, Supervision, Conceptualization. **Leung Christopher KY:** Writing – review & editing, Supervision, Funding acquisition, Conceptualization. **Haroon Younas:** Writing – original draft, Investigation, Formal analysis, Data curation.

Declaration of Competing Interest

The authors declare that they have no known competing financial interests or personal relationships that could have appeared to influence the work reported in this paper.

Acknowledgements

This study was supported by Hong Kong Research Grants Council (16211617, 16204421) and National Natural Science Foundation of China (52108264, 52211530099). The first author also acknowledges the Hong Kong PhD Fellowship.

Data Availability

Data will be made available on request.

References

[1] P. Domone, M. Soutsos, Construction materials: their nature and behaviour: fifth edition, construction materials, Their Nat. Behav.: Fifth Ed. (2017) 1–820, https://doi.org/10.1201/9781315164595.
[2] D. Dackman, C.G. Berrocal, R. Rempling, I. Fernandez, A framework for evaluating steel loss from the evolution of corrosion-induced deflections in reinforced concrete beams with non-uniform reinforcement corrosion, Eng. Struct. 317 (2024) 118593, https://doi.org/10.1016/J.ENGSTRUCT.2024.118593.
[3] G. Malumbela, M. Alexander, P. Moyo, Steel corrosion on RC structures under sustained service loads — a critical review, Eng. Struct. 31 (2009) 2518–2525, https://doi.org/10.1016/J.ENGSTRUCT.2009.07.016.
[4] A.K. El-Sayed, Shear capacity assessment of reinforced concrete beams with corroded stirrups, Constr. Build. Mater. 134 (2017) 176–184, https://doi.org/10.1016/j.conbuildmat.2016.12.118.
[5] R. Mourão, A. Caçoilo, F. Teixeira-Dias, D. Lecompte, T. Stratford, Concrete plates with externally bonded FRP under contact detonations, Constr. Build. Mater. 310 (2021) 125073, https://doi.org/10.1016/J.CONBUILDMAT.2021.125073.
[6] P. Li, J. Zeng, W. Li, Y. Zhao, Effect of concrete heterogeneity on interfacial bond behavior of externally bonded FRP-to-concrete joints, Constr. Build. Mater. 359 (2022) 129483, https://doi.org/10.1016/J.CONBUILDMAT.2022.129483.
[7] I. Shaw, B. Andrawes, Repair of damaged end regions of PC beams using externally bonded FRP shear reinforcement, Constr. Build. Mater. 148 (2017) 184–194, https://doi.org/10.1016/J.CONBUILDMAT.2017.05.077.
[8] J.P. Lin, Y.F. Wu, S.T. Smith, Width factor for externally bonded FRP-to-concrete joints, Constr. Build. Mater. 155 (2017) 818–829, https://doi.org/10.1016/J.CONBUILDMAT.2017.08.104.
[9] R. Kotynia, Bond between FRP and concrete in reinforced concrete beams strengthened with near surface mounted and externally bonded reinforcement, Constr. Build. Mater. 32 (2012) 41–54, https://doi.org/10.1016/J.CONBUILDMAT.2010.11.104.
[10] J.R. Cromwell, K.A. Harries, B.M. Shahrooz, Environmental durability of externally bonded FRP materials intended for repair of concrete structures, Constr. Build. Mater. 25 (2011) 2528–2539, https://doi.org/10.1016/J.CONBUILDMAT.2010.11.096.
[11] H. Guo, H.H. Liao, M. Su, B. Zhang, S. Li, H. Peng, Shear strengthening of RC beams with prestressed NSM CFRP: influencing factors and analytical model, Compos Struct. 342 (2024) 118262, https://doi.org/10.1016/J.COMPSTRUCT.2024.118262.
[12] M.J. Jedrzejko, S.S. Zhang, Y. Ke, D. Fernando, X.F. Nie, Shear strengthening of RC beams with NSM FRP. I: review of strength models, Adv. Struct. Eng. 26 (2023) 564–586, https://doi.org/10.1177/13694332221125832.
[13] M. Ibrahim, T. Wakjira, U. Ebead, Shear strengthening of reinforced concrete deep beams using near-surface mounted hybrid carbon/glass fibre reinforced polymer strips, Eng. Struct. 210 (2020), https://doi.org/10.1016/j.engstruct.2020.110412.

[14] S.S. Zhang, M.J. Jedrzejko, Y. Ke, T. Yu, X.F. Nie, Shear strengthening of RC beams with NSM FRP strips: concept and behaviour of novel FRP anchors, Compos Struct. 312 (2023) 116790, https://doi.org/10.1016/J.COMPSTRUCT.2023.116790.
[15] W. Lu, Z. Ling, Q. Geng, W. Liu, H. Yang, K. Yue, Study on flexural behaviour of glulam beams reinforced by near surface mounted (NSM) CFRP laminates, Constr. Build. Mater. 91 (2015) 23–31, https://doi.org/10.1016/J.CONBUILDMAT.2015.04.050.
[16] O. Aljidda, A. El Refai, W. Alnahhal, Comparative study on the bond performance of near-surface mounted fiber-reinforced polymer bars, Constr. Build. Mater. 364 (2023) 129923, https://doi.org/10.1016/J.CONBUILDMAT.2022.129923.
[17] I.A. Sharaky, A.S. Elamary, Y.M. Alharthi, Experimental and numerical investigation on the flexural performance of RC slabs strengthened with EB/NSM CFRP reinforcement and bonded reinforced HSC layers, Eng. Struct. 289 (2023), https://doi.org/10.1016/j.engstruct.2023.116338.
[18] L. De Lorenzis, J.G. Teng, Near-surface mounted FRP reinforcement: an emerging technique for strengthening structures, Compos B Eng. 38 (2007) 119–143, https://doi.org/10.1016/j.compositesb.2006.08.003.
[19] S. Gopinath, A.R. Murthy, H. Patrawala, Near surface mounted strengthening of RC beams using basalt fiber reinforced polymer bars, Constr. Build. Mater. 111 (2016) 1–8, https://doi.org/10.1016/j.conbuildmat.2016.02.046.
[20] Y. Taleb Obaidat, W. Barham, R.B. Obeidat, Repair of thermally shocked reinforced concrete beams using near-surface mounted – carbon fiber reinforced polymers ropes and strips, Constr. Build. Mater. 366 (2023) 130201, https://doi.org/10.1016/J.CONBUILDMAT.2022.130201.
[21] W. Miao, Z.X. Guo, Y. Ye, S. Humayun Basha, Shear behavior of composite stone beams reinforced with NSM longitudinal CFRP bars, Constr. Build. Mater. 363 (2023) 129802, https://doi.org/10.1016/J.CONBUILDMAT.2022.129802.
[22] J.F. Chen, J.G. Teng, Anchorage strength models for frp and steel plates bonded to concrete, J. Struct. Eng. 127 (2001) 784–791, https://doi.org/10.1061/(ASCE)0733-9445(2001)127:7(784).
[23] J.G. Teng, J.F. Chen, S.T. Smith, L. Lam, FRP: Strengthened RC Structures, Wiley, 2002.
[24] TC Triantafillou, Shear strengthening of reinforced concrete beams using epoxy-bonded FRP composites, Acids Struct. J. 95 (1998).
[25] A.M. Malek, H. Saadatmanesh, M.R. Ehsani, Prediction of bond strength of externally bonded FRP sheets, J. Compos. Constr. 2 (4) (1998) 186–191.
[26] L. De Lorenzis, E. Zurich, C. Modena, A. Nanni, Bond between near-surface mounted fiber-reinforced polymer rods and concrete in structural strengthening, Acids Struct. J. 99 (2) (2002) 123–132.
[27] G. Monti, M.A. Liotta, S. Matthys, Performance of near-surface mounted CFRP strips for strengthening concrete beams, J. Compos. Constr. 7 (2) (2003) 93–101.
[28] L. De Lorenzis, J.G. Teng, Near-surface mounted FRP reinforcement: an emerging technique for strengthening structures, Compos B Eng. 38 (2007) 119–143, https://doi.org/10.1016/J.COMPOSITESB.2006.08.003.
[29] R. Fico, G. Spadea, A. Nanni, Strengthening of concrete structures with NSM CFRP strips, Compos B Eng. 39 (6) (2008) 1046–1053.
[30] G. Van Zijl, V. Slowik, A framework for durability design with strain-hardening cement-based composites (SHCC) (-FDS), State—Art. Rep. RILEM Tech. Comm. (2017) 240 (-FDS).
[31] J. Yu, Y. Chen, C.K.Y. Leung, Mechanical performance of Strain-Hardening Cementitious Composites (SHCC) with hybrid polyvinyl alcohol and steel fibers, Compos Struct. 226 (2019) 111198, https://doi.org/10.1016/J.COMPSTRUCT.2019.111198.
[32] V.C. Li, Engineered Cementitious Composites (ECC): bendable concrete for sustainable and resilient infrastructure, SPRINGER Nat. 1 (2019) 419, https://doi.org/10.1007/978-3-662-58438-5/COVER.
[33] B. Pan, F. Liu, Y. Zhuge, J.J. Zeng, J.J. Liao, ECCs/UHPFRCCs with and without FRP reinforcement for structural strengthening/repairing: a state-of-the-art review, Constr. Build. Mater. 316 (2022) 125824, https://doi.org/10.1016/J.CONBUILDMAT.2021.125824.
[34] V. Mechtcherine, Novel cement-based composites for the strengthening and repair of concrete structures, Constr. Build. Mater. 41 (2013) 365–373, https://doi.org/10.1016/J.CONBUILDMAT.2012.11.117.
[35] M. Luković, H. Dong, B. Šavija, E. Schlangen, G. Ye, K.Van Breugel, Tailoring strain-hardening cementitious composite repair systems through numerical experimentation, Cem. Concr. Compos 53 (2014) 200–213, https://doi.org/10.1016/J.CEMCONCOMP.2014.06.017.
[36] J. Yu, H. Li, C.K.Y. Leung, X. Lin, J.Y.K. Lam, I.M.L. Sham, K. Shih, Matrix design for waterproof engineered cementitious composites (ECCs), Constr. Build. Mater. 139 (2017) 438–446, https://doi.org/10.1016/J.CONBUILDMAT.2017.02.076.
[37] X. Yang, W.Y. Gao, J.G. Dai, Z.D. Lu, Shear strengthening of RC beams with FRP grid-reinforced ECC matrix, Compos Struct. 241 (2020) 112120, https://doi.org/10.1016/J.COMPSTRUCT.2020.112120.
[38] Z. Zhang, D. Liu, J.A. Abdalla, R.A. Hawileh, F. Qin, X. Xu, Flexural behavior of reinforced concrete beams externally strengthened with ECC and FRP grid reinforcement, Constr. Build. Mater. 446 (2024) 137964, https://doi.org/10.1016/J.CONBUILDMAT.2024.137964.
[39] L. Cong, F. Zhang, Y. Qian, Experimental and theoretical study on ECC-CFRP jointly flexural reinforcement of pre-damaged reinforced concrete beams, Constr. Build. Mater. 444 (2024) 137720, https://doi.org/10.1016/J.CONBUILDMAT.2024.137720.
[40] M. Ellithy, A. Hassan, T.F. El-Shafiey, Flexural strengthening of RC beams using PGFRP bars embedded in strain-hardening cementitious composites (SHCC), Eng. Struct. 317 (2024) 118628, https://doi.org/10.1016/J.ENGSTRUCT.2024.118628.
[41] Y. Chen, J. Yu, C.K.Y. Leung, Use of high strength Strain-Hardening Cementitious Composites for flexural repair of concrete structures with significant steel corrosion, Constr. Build. Mater. 167 (2018) 325–337, https://doi.org/10.1016/j.conbuildmat.2018.02.009.
[42] T.C.S.P. Figueiredo, M. Hering, I. Curosu, F. Bracklow, S. Scheerer, M. Curbach, V. Mechtcherine, F. de A. Silva, Effect of shear reinforcement and external strengthening with strain-hardening cement-based composites (SHCC) on the impact resistance of reinforced concrete beams, Cem. Concr. Compos 145 (2024) 105371, https://doi.org/10.1016/J.CEMCONCOMP.2023.105371.
[43] A.T. Baraghith, A.H.A. Khalil, E.E. Etman, R.N. Behiry, Improving the shear behavior of RC dapped-end beams using precast strain-hardening cementitious composite (P-SHCC) plates, Structures 50 (2023) 978–997, https://doi.org/10.1016/J.ISTRUC.2023.02.059.
[44] Z. Hu, Y. Zhou, B. Hu, X. Huang, M. Guo, Local use of ECC to simultaneously enhance the shear strength and deformability of RC beams, Constr. Build. Mater. 353 (2022) 129085, https://doi.org/10.1016/J.CONBUILDMAT.2022.129085.
[45] T.C.S.P. Figueiredo, C.M.R. Gaspar, M. Hering, I. Curosu, M. Curbach, V. Mechtcherine, F. de Andrade Silva, Experimental modal analysis of RC beams strengthened with SHCC subjected to shear under impact strain rates, Eng. Struct. 264 (2022) 114459, https://doi.org/10.1016/J.ENGSTRUCT.2022.114459.
[46] S. He, S. Mustafa, Z. Chang, M. Liang, E. Schlangen, M. Luković, Ultra-thin Strain Hardening Cementitious Composite (SHCC) layer in reinforced concrete cover zone for crack width control, Eng. Struct. 292 (2023) 116584, https://doi.org/10.1016/J.ENGSTRUCT.2023.116584.
[47] C.C. Hung, Y.S. Chen, Innovative ECC jacketing for retrofitting shear-deficient RC members, Constr. Build. Mater. 111 (2016) 408–418, https://doi.org/10.1016/J.CONBUILDMAT.2016.02.077.
[48] A. Hassan, A.T. Baraghith, A.M. Atta, T.F. El-Shafiey, Retrofitting of shear-damaged RC T-beams using U-shaped SHCC jacket, Eng. Struct. 245 (2021) 112892, https://doi.org/10.1016/J.ENGSTRUCT.2021.112892.
[49] Y.Z. Zheng, W.W. Wang, K.M. Mosalam, Q. Fang, L. Chen, Z.F. Zhu, Experimental investigation and numerical analysis of RC beams shear strengthened with FRP/ECC composite layer, Compos Struct. 246 (2020) 112436, https://doi.org/10.1016/J.COMPSTRUCT.2020.112436.
[50] A. Zheng, S. Li, D. Zhang, Y. Yan, Shear strengthening of RC beams with corrosion-damaged stirrups using FRP grid-reinforced ECC matrix composites, Compos Struct. 272 (2021) 114229, https://doi.org/10.1016/J.COMPSTRUCT.2021.114229.
[51] C. Wu, V.C. Li, CFRP-ECC hybrid for strengthening of the concrete structures, Compos Struct. 178 (2017) 372–382, https://doi.org/10.1016/J.COMPSTRUCT.2017.07.034.
[52] W. Hou, Z.Q. Li, W.Y. Gao, P.D. Zheng, Z.X. Guo, Flexural behavior of RC beams strengthened with BFRP bars-reinforced ECC matrix, Compos Struct. 241 (2020) 112092, https://doi.org/10.1016/J.COMPSTRUCT.2020.112092.
[53] B. Pan, F. Liu, Y. Zhuge, J.J. Zeng, J.J. Liao, ECCs/UHPFRCCs with and without FRP reinforcement for structural strengthening/repairing: a state-of-the-art review, Constr. Build. Mater. 316 (2022), https://doi.org/10.1016/j.conbuildmat.2021.125824.
[54] G. Fischer, V.C. Li, Influence of Matrix Ductility on Tension-Stiffening Behavior of Steel Reinforced Engineered Cementitious Composites (ECC), (2002). ⟨http://hdl.handle.net/2027.42/84804⟩.
[55] K. Otsuka, H. Mihashi, M. Kiyota, S. Mori, A. Kawamata, Observation of multiple cracking in hybrid FRCC at micro and meso levels, J. Adv. Concr. Technol. 1 (2003) 291–298, https://doi.org/10.3151/jact.1.291.
[56] Y. Chen, J. Yu, H. Younas, C.K.Y. Leung, Experimental and numerical investigation on bond between steel rebar and high-strength Strain-Hardening Cementitious Composite (SHCC) under direct tension, Cem. Concr. Compos 112 (2020) 103666, https://doi.org/10.1016/j.cemconcomp.2020.103666.
[57] H. Younas, J. Yu, C.K. Leung, Mechanical and environmental performance of high-strength strain-hardening cementitious composites with high-dosage ternary supplementary cementitious materials: fly ash, limestone, and calcined clay, Constr. Build. Mater. 444 (2024) 137856, https://doi.org/10.1016/J.CONBUILDMAT.2024.137856.
[58] D. Zhang, J. Yu, H. Wu, B. Jaworska, B.R. Ellis, V.C. Li, Discontinuous micro-fibers as intrinsic reinforcement for ductile engineered cementitious composites (ECC), Compos B Eng. 184 (2020) 107741.
[59] L.-Y. Xu, J. Yu, B.-T. Huang, J.-C. Lao, H.-L. Wu, X. Jiang, T.-Y. Xie, J.-G. Dai, Green and low-carbon matrices for engineered/strain-hardening cementitious composites (ECC/SHCC): toward sustainable and resilient infrastructure, J. Clean. Prod. 496 (2025) 144968, https://doi.org/10.1016/J.JCLEPRO.2025.144968.
[60] Construction Standard CS2:2012 - Steel Reinforcing Bars for the Reinforcement of Concrete (June 2022). The Government of the Hong Kong Special Administrative Region (2022).
[61] J. Yu, H.L. Wu, D.K. Mishra, G. Li, C.K. Leung, Compressive strength and environmental impact of sustainable blended cement with high-dosage Limestone and Calcined Clay (LC2), J. Clean. Prod. 278 (2021) 123616, https://doi.org/10.1016/J.JCLEPRO.2020.123616.
[62] J. Yu, H.-L. Wu, C.K.Y. Leung, Feasibility of using ultrahigh-volume limestone-calcined clay blend to develop sustainable medium-strength Engineered

Cementitious Composites (ECC), J. Clean. Prod. 262 (2020) 121343, https://doi.org/10.1016/j.jclepro.2020.121343.
[63] H. Younas, J. Yu, C.K.Y. Leung, Effect of bar diameter and cover thickness on bond behavior of steel bar in high-strength SHCC under pull-out condition: Experimental study and efficient finite element modeling, J. Build. Eng. 105 (2025) 112471, https://doi.org/10.1016/J.JOBE.2025.112471.
[64] J. Wei, C. Wu, Y. Chen, C.K.Y. Leung, Shear strengthening of reinforced concrete beams with high strength strain-hardening cementitious composites (HS-SHCC), Mater. Struct. 53 (2020), https://doi.org/10.1617/s11527-020-01537-1.
[65] W. Ren, L. Sneed, Y. Yang, R. He, Numerical simulation of prestressed precast concrete bridge deck panels using damage plasticity model, Int J. Concr. Struct. Mater. 9 (2015) 45–54, https://doi.org/10.1007/s40069-014-0091-2.
[66] K.E. Barth, H. Wu, Efficient nonlinear finite element modeling of slab on steel stringer bridges, Finite Elem. Anal. Des. 42 (2006) 1304–1313, https://doi.org/10.1016/j.finel.2006.06.004.